TLU 15/73

LOW-ENERGY PROTON INDUCED DEUTERON BREAKUP ANALYZED WITH THE SEPARABLE POTENTIAL MODEL

B Sundqvist and A Johansson

Tandem Accelerator Laboratory

Box 533

S-751 21 Uppsala, Sweden, tel 018/10 04 70

TLU 15/73
April 1973

LOW-ENERGY PROTON INDUCED DEUTERON BREAKUP ANALYZED WITH THE SEPARABLE POTENTIAL MODEL

Bo Sundqvist and Arne Johansson

Tandem Accelerator Laboratory, Uppsala, Sweden

ABSTRACT

Experimental data from low-energy proton induced deuteron breakup have been analyzed with the separable potential model (SPM). The experimental data cover symmetric and asymmetric coplanar correlations and symmetric noncoplanar correlations at T_p = 10.0 MeV measured at this laboratory and symmetric coplanar correlations at T_p = 12.5 MeV measured at Rice University. The agreement between the SPM calculations of and experimental data on the correlation spectra is very good both in shape and absolute magnitude. However, systematic deviations between experimental data and SPM predictions for kinematic conditions corresponding to low relative pp energy are found, at least partly due to the neglect of Coulomb effects in the pp interaction used in the calculations. A review of the SPM model is given.

This work was supported by the Swedish Atomic Research Council

1. INTRODUCTION

In the last decade much interest has been devoted to the three-nucleon problem. One of the reasons is the important theoretical progress made by Faddeev[1] who in 1960 formulated the integral equations giving an exact quantum mechanical description of the three-body system. Later Mitra[2], Lovelace[3] and Amado[4] have made important contributions to the solution of the three-body scattering problem using separable two-body forces. From the experimental point of view the incorporation of on-line computers and efficient multiparameter data collection systems in the experimental facilities has made it possible to perform accurate and kinematically complete experiments mapping large parts of the phase space in three-nucleon reactions. Early theoretical attempts to describe the deuteron breakup by neutrons or protons concentrated on the two-body aspects of the reactions, i. e. the first two terms in the multiple scattering formula[5,6,7]. The idea in most experiments has been to isolate a certain reaction mechanism by a careful choice of kinematics. The spectator model[6] has been applied to cases where one of the nucleons is left with a low energy in the laboratory and the Migdal-Watson theory[8] for final state interactions to kinematical regions where the internal energy of a pair of nucleons is low in the final state. For high incident energies ($T_{n,p} > 100$ MeV) these kinematic regions are rather well separated and the multiple scattering series probably converges and the models give a fairly good description of the experimental data[6]. For lower incident energies the phase space becomes narrower and a clean separation is hardly possible to achieve[9]. Also, the multiple scattering series may not converge[10].

In four recent reports from this laboratory[11,12,13,14] an experimental investigation of the peak corresponding to low neutron energy in the d(p,2p)n reaction at $T_p = 10.0$ MeV was presented. This peak is by tradition called the "quasifree" pp-scattering peak. The spectator model has been used to analyze most experiments even at low energy[9,15]. From different experiments at this laboratory it was found that some of the earlier statements made on the origin of the "quasifree" peak are justified mainly because all earlier experiments on this peak at low energy ($T_p < 13$ MeV) have been performed in a symmetric coplanar geometry[9,15]. On the contrary in the asymmetric coplanar[11] cases the position of the "quasifree" peak no longer

occurs at minimum neutron energy but rather at equal internal energies in the two pn systems possible. Furthermore a Treiman-Yang test[12] showed that it was unlikely that the spectator diagram dominates the process. Also an investigation of the noncoplanar correlations[13] in the d(p,2p)n reaction clearly showed the failure of the spectator model to account for the experimental data. Finally, an attempt to include pn quasifree scattering and final state interaction corrections in the calculations using the procudure given by Cromer, Thorndike and Brown gave very poor agreement with experiment[14], indicating the need for an exact treatment taking all three nucleons into account.

Amado[4], Cahill[16], Ebenhöh[17] and others have used separable interactions for the two-body forces and succeeded in solving the integral equations numerically. The two-body forces were spin-dependent, s-wave, Yamaguchi interactions. Coulomb forces have so far not been included. Also hard core and higher partial waves in the two-body interactions have to be included in the calculations before any conclusions can be made about specific three-body effects such as off-energy-shell effects and three-body forces. Using Ebenhöh's* computer codes experimental data on proton induced deuteron breakup obtained at Uppsala[11,13] have been analyzed. Experiments at higher proton energies ($T_p \geq 13.5$ MeV) have previously been compared with similar calculations[17,18,19]. Data at lower energies may be more relevant because of the neglect of higher partial waves than the s-waves in the two-body interactions used in the calculations.

The agreement in spectrum shape as well as in absolute magnitude between calculation and experiment gives rise to a hope that more detailed comparisons might yield information on off-energy-shell effects or three-nucleon forces provided the calculation can be refined to include the Coulomb force and phase equivalent two-nucleon interactions. Several requirements will also be put on the experimental accuracy. Therefore, an effort was made to determine the absolute cross section scale and some additional spectra were obtained with better statistics than previously (section 2). For the sake of completeness, a short review of the fundamental relations in the calculations is given in sect 3. In section 4 the calculations are compared with data at $T_p = 10.0$ MeV obtained at Uppsala and with data from Rice University at $T_p = 12.5$ MeV[15].

---

* We are very grateful to Dr Ebenhöh for sending us his computer codes

2. EXPERIMENTAL CONSIDERATIONS

The coplanar correlation measurements at Uppsala[11] were made with rather poor statistics and therefore a few additional, representative spectra have been obtained with better accuracy for comparison with the separable potential model (SPM) calculations. The additional spectra obtained at T_p = 10.0 MeV covered the following angular settings: a) symmetric coplanar, $\theta_3 = \theta_4$ = 30.0° and 36.7°; and b) asymmetric-coplanar, θ_3 = 30.0°, θ_4 = 43.4° and 75.4°. The spectra were obtained with the same procedure as the one described in ref 11 except for a few changes described below.

Due to the complexity of the total system of accelerator, scattering chamber, detectors, electronics and computer various check procedures must be used during the experiment, It is important to reveal and replace a failing component as soon as possible and because of such a failure reject doubtful data. The different precautions described below represent such check procedures. The main effort concerned the determination of absolute cross sections.

In the earlier measurements the largest contribution to the uncertainty in the cross section measurement came from the determination of the solid angles. The largest source of error was probably the deformation of the deuterated polyethylene target due to beam heating. For this reason a device to rotate the target was constructed (Fig 1). This device was run with a speed of 20 turns per minute and used to check the experimental set up and look for drifts which might influence the absolute cross section scale. It was found that the target deformations were smaller than earlier and that the combined uncertainty in the solid angle determination was now 0.8 % rather than the previous[11] 1.6 %. This number could probably be further improved by the use of polyethylene targets with carbon backing.

In the check run discussed above, a spectrum for T_p = 10.0 MeV ($\theta_3 = \theta_4$ = 30.0°; φ_3 = 0.0° and φ_4 = 180.0°) was measured. It was separated into four parts. The extracted cutoff radii were 5.52 ± 0.16; 5.52 ± 0.14; 5.51 ± 0.10 and 5.64 ± 0.14 fm. During the run elastically scattered protons from deuterium were counted both in the coincidence and in the two monitor detectors (θ_{M1} = 54.8° and θ_{M2} = 60.0°). The ratios between these numbers in the four spectra were compared with the same ratios calculated from

known elastic pd cross sections[20] and solid angles. The agreement was good.

In Table II a summary of cutoff radii determined at Uppsala for the same kinematic situation is given. The measurements involved different targets, solid angles (target to detector distance and aperture diameter), beam characteristics (beam current, beam-spot diameter), and electronics. The agreement is acceptable. In all measurements reported from this laboratory on this reaction[11,12,13], a data taking period was always started and concluded with this spectrum.

A very important check on the absolute cross section scale was the experiment performed to remeasure the elastic pd cross section at 10.0 MeV[21]. It was shown that the reference data used previously on elastic pd scattering by A C Wilson et al[20] were 10 % to small. Consequently all cross-sections in this report for data obtained at Uppsala were renormalized with a factor 1.10. However, all cutoff radii refer to the old cross section scale.

3. THEORETICAL BACKGROUND TO THE CALCULATIONS

An excellent treatment of nonrelativistic three-particle scattering has been given by I Duck[22] and most of the notations used below were taken from this review. Klein[18] has also reviewed the background to Ebenhöh's calculations in his thesis.

3.1 Two-body scattering

Two-body scattering is usually described with the Lippman-Schwinger equation. The main advantage of this integral equation over the Schrödinger equation technique is that the boundary conditions for large distances between the interacting particles is built into the equation. The Schrödinger equation for two-body scattering can be written in the following way, when the potential is assumed to be spherically symmetric, independent of spin and of finite range:

$$(H_o - E_k)\,\psi_k = -V\psi_k$$
$$\{E_k = \frac{k^2}{2m} \;:\; H_o = -\frac{\nabla^2}{2m}\} \qquad (1)$$

Formally one can write the solution as

$$\psi_k = \phi_k - \frac{1}{H_o - E_k} V\psi_k \qquad (2)$$

where ϕ_k is the solution of the homogenous equation with $V = 0$

E^+ is defined through

$$E^+ = E + i\eta \qquad (3)$$

where it is understood that η is a small positive quantity which eventually will approach zero.

The operator in (2) is the free two-particle Green's function

$$g_o(E) = (H_o - E^+)^{-1} \qquad (4)$$

and equation (2) can then be written

$$\psi = \phi - g_o V\psi \qquad (5)$$

By iteration it can be shown

$$\psi = \phi - gV\phi \qquad (6)$$

where

$$g = g_o - g_o V g_o + \ldots = (1 + g_o V)^{-1} g_o \tag{7}$$

A complete knowledge of the full Green's function g is equivalent to a solution of the scattering problem.

It can be shown that

$$\psi = \lim_{\eta \to 0^+} - i\eta g \phi \tag{8}$$

From the definition of the t-matrix an equation similar to (5) can be derived

$$t = V - V g_o t \tag{9}$$

This is the Lippman-Schwinger equation for the t-matrix.

By iteration it can be shown that

$$t = V - V g V \tag{10}$$

Once again it follows that the knowledge of the full Green's function is equivalent to a solution of the scattering problem.
The Lippman-Schwinger equation (8) has a unique solution if the kernel ($K = g_o V$) is compact, i.e. square integrable, which can be shown to be true if the potential itself is square integrable, or

$$\int V^2(r)\, d^3r < \infty \tag{11}$$

3.2 Three-body scattering

In three-body scattering there are two major complications compared to two-body scattering. The number of degrees-of-freedom increases. In two-body scattering, one relative momentum vector is enough for a complete specification but in three-body scattering one needs two relative momentum vectors. For example, particle 1 has the momentum $\vec{p}_1$ relative to the center-of-mass of the subsystem (2,3) and this subsystem has the momentum $\vec{k}_1$ relative to the total center-of-mass. This means that even after a partial wave decomposition of the amplitudes, the integral equations are coupled integral equations for functions of two variables.

Another important complication arises if one tries to use the Lippman-Schwinger equation to formulate the three-particle scattering problem.

The three particle Green's function G is defined by

$$G = G_o - G_o V G \tag{12}$$

where $V = V_1 + V_2 + V_3$ is the total interaction between the three particles. V_1 is the interaction between pair (2,3) and G_o is the free three particle Green's function

$$G_o = (H_o - E^+)^{-1} \text{ with } H_o = \frac{p_1^2}{2m_1} + \frac{p_2^2}{2m_2} + \frac{p_3^2}{2m_3}$$

The kernel $G_o V$ will thus contain terms of the type

$$\delta^3(\vec{p}_1 - \vec{p}_1') < \vec{p}_2 \vec{p}_3 \, |V_1| \, \vec{p}_2' \vec{p}_3' > \tag{13}$$

Now the integral of a squared δ-function is infinite and consequently the kernel will not be compact. Then the Lippman-Schwinger equation will not give unique solutions.

Faddeev[1] solved this problem in an elegant way. He wrote down a system of coupled integral equations each of which had a compact kernel. Faddeev began his derivation by writing down the complete Green's function in terms of an operator T

$$G = G_o - G_o T G_o \tag{14}$$

so that T satisfies

$$T = V - V G_o T \tag{15}$$

The terms generated by iterating this equation are

$$T = V_1 + V_2 + V_3 - (V_1 + V_2 + V_3)G_o(V_1 + V_2 + V_3) + \ldots = \\ = V_1 - V_1G_oV_1 - V_1G_oV_2 - V_1G_oV_3 + V_2 - V_2G_oV_2 - \ldots \tag{16}$$

where various subseries can be identified

$$T = t_1 + t_2 + t_3 - t_1G_ot_2 - t_1G_ot_3 + \ldots \tag{17}$$

where

$$t_i = V_i - V_iG_ot_i \tag{18}$$

Faddeev recognized these series as terms in an integral equation for T

$$T = T_1 + T_2 + T_3 \tag{19}$$

where

$$\begin{cases} T_1 = t_1 - t_1 G_o (T_2 + T_3) \\ T_2 = t_2 - t_2 G_o (T_1 + T_3) \\ T_3 = t_3 - t_3 G_o (T_1 + T_2) \end{cases} \qquad \tilde{T}_i = \tilde{t}_i + \tilde{K}\tilde{T} \tag{20}$$

and

$$\tilde{K} = \begin{Bmatrix} 0 & t_1 & t_1 \\ t_2 & 0 & t_2 \\ t_3 & t_3 & 0 \end{Bmatrix} \tag{21}$$

Faddeev has shown that this (Faddeev) kernel $\tilde{K}$ is compact or can be made compact which means that the solutions to the Faddeev equations are unique. The structure of the equations shows that T_i corresponds to the pair i interacting last. Faddeevs work is considered as the first paper in which a mathematically correct nonrelativistic three-particle theory was presented. It has often been stated that these integral equations are rather unpractical to use in calculations. However, contributions of Lovelace[3], Amado[4], Sandhaz[23] and others have given modifications of the Faddeev approach, more practical for numerical calculations. The calculations by Ebenhöh which are used in this work are closely connected with the work of Sandhaz and collaboraters[23].

The starting point is Faddeev-like equations for appropriately chosen transition operators ($U_{\alpha\beta}$). Here α and β refer to the channel definition for

three-body scattering given by Ekstein[24].

$$U_{\alpha\beta} = -(1-\delta_{\alpha\beta})G_o - \sum_{\delta\neq\alpha} U_{\alpha\delta}\, G_o\, t_\delta \qquad (22)$$

These are reduced to multichannel two-particle Lippman-Schwinger equations. The advantage of this procedure is that $U_{\alpha\beta}$ are directly connected to the S-matrix elements

$$S_{\beta n,\,\alpha m} = \delta_{\beta\alpha}\,\delta_{nm} - 2\pi i\delta\,(E_{\beta n} - E_{\alpha m}) < \phi_{\beta n}|U_{\beta\alpha}|\phi_{\alpha m} > \qquad (23)$$

and that t_δ are related to the two particle t-matrix. Here $\vec{p}_\delta$ is the momentum of a pair δ relative to the total center-of-mass and $\vec{q}_\delta$ is the momentum of the third particle relative the center-of-mass of the pair δ.

$$\begin{aligned} &(<\vec{p}_\delta|\hat{t}_\delta|\vec{p}_\delta'> = t_\delta(\vec{p}_\delta, \vec{p}_\delta', E)) \\ &<\vec{p}_\delta, \vec{q}_\delta|t_\delta|\vec{p}_\delta', \vec{q}_\delta'> = \delta(\vec{q}_\delta - \vec{q}_\delta') <\vec{p}_\delta|\hat{t}_\delta \\ &(E - \vec{q}_\delta^{\,2})\ |\vec{p}_\delta'> \end{aligned} \qquad (24)$$

This also shows that the t-matrix element must be known off the energy shell. However, the coupled integral equations are associated with two continous variables (p,q) and numerical solutions are in most cases too complicated to achieve. It was early suggested by Mitra[2], Lovelace[3] and Amado[4] that this problem could be overcome by the use of separable two-body interactions.

3.3 SEPARABLE TWO-BODY INTERACTIONS

An example of a separable interaction is a separable potential V. In momentum space one can write

$$\langle \vec{k}|V|\vec{k}' \rangle = \lambda v(k) \cdot v(k') \tag{25}$$

and the corresponding t-matrix element is

$$\langle \vec{k}|t(E)|\vec{k}' \rangle v(k)\tau(E)v(k') \tag{26}$$

where $\tau(E)$ is the two-particle propagator[17].

Amado[25] has illustrated the use of a separable two-body interaction when three-particles are considered. In Fig 2a an arbitrary three-body amplitude (two-body scattering while the third is going by) is shown and Fig 2b shows the corresponding diagram when a separable two-body interaction is used. At the dashed line the three-body state has two-body kinematics. What enters into the three-body amplitudes are not the potentials but the off-shell t-matrix elements as indicated in section 3.2 and these are not simply related to the potential form. If a two-body bound state, virtual state or resonance pole dominates the two-body amplitude the separable form is an excellent approximation to that amplitude. This can for example be seen in Fig 2 where the separable form makes the scattering to through a particle-like (quasi particle) intermediate state for which $\tau(E)$ is the propagator.

However, at first sight it might seem unjustified to use a separable potential since for large distances field theoretical potentials are local and nonseparable. Lovelace[3] argued that one of the most important results of the Faddeev theory is that it justifies the use of separable potentials and that the condition for it to be valid is that the two-particle subsystem shall be dominated by a limited number of bound states and resonances. This should be well fulfilled for the p + d system with s-wave scattering in the S = 1 state with a pole at the binding energy of the deuteron and in the S = 0 state with virtual states near zero energy in the T = 1 isospin triplet (nn; np; pp).

Ebenhöh[17] used spin dependent s-wave Yamaguchi two-body forces

$$v(p', p) = \lambda g(p')g(p) \tag{27}$$

where $g(p)$ is the Yamaguchi form factor[26]

$$g(p) = \frac{N}{p^2 + \beta^2} \tag{28}$$

and N is a normalization constant given in ref 17.

The propagator $\tau(E)$ is

$$\tau(E) = \frac{J(\sqrt{\epsilon})}{k + i\sqrt{\epsilon}} \tag{29}$$

where J is a Jost function. The parameters k and β are connected with the scattering length (a) and the effective range (r_o) through the relations

$$\begin{aligned} &(k + \beta)^2(r_o\beta - 1) - 2\beta^2 = 0 \\ &(k - \tfrac{1}{2}r_o k^2) = \frac{1}{a} \end{aligned} \tag{30}$$

The effective range parameters used in the calculations are given in Table I. The two-body forces used are rather uncomplicated. Especially the lack of Coulomb forces is an important limitation as will be shown below. Also hard cores, tensor forces and higher partial waves are important to include in the calculation. At 10 MeV, i.e. the energy of the present data, the last three features of the two-body interaction should not be too important.

3.4 THE EBENHÖH PROGRAMME

Ebenhöh[17] has given a detailed description of his calculations. After formulating the integral equations for the breakup amplitude, he considered the spin algebra and the necessary antisymmetrization. The three particle states have the form $|p_i, q_i, \sigma_i, S, T, M_S, M_T\rangle$. As only s-wave interactions are involved the total spin S is not coupled to the angular momentum. The total isospin T is also fixed to $T = \frac{1}{2}$ ($T_d = 0$). $\sigma_i = (S_i, T_i)$ denotes the spin-isospin state of pair i. Only interactions in the cases (1;0) and (0;1) are assumed.

$T^S_{(S_i, T_i)}(p,q)$ are the amplitudes which form the total amplitude

$$|T_N|^2 = \frac{1}{9}\{T^{\frac{1}{2}}_{(0,1)}(1) + \frac{1}{4}(T^{\frac{1}{2}}_{(0,1)}(2) + T^{\frac{1}{2}}_{(0,1)}(3)) - \frac{3}{4}(T^{\frac{1}{2}}_{(1,0)}(2) + T^{\frac{1}{2}}_{(1,0)}(3))\}^2$$

$$+ \frac{1}{9}\{\frac{\sqrt{3}}{4}(T^{\frac{1}{2}}_{(0,1)}(2) - T^{\frac{1}{2}}_{(0,1)}(3)) + \frac{\sqrt{3}}{4}(T^{\frac{1}{2}}_{(1,0)}(2) - T^{\frac{1}{2}}_{(1,0)}(3))^2$$

$$+ \frac{2}{9}\{\frac{\sqrt{3}}{2}(T^{\frac{3}{2}}_{(1,0)}(2) - T^{\frac{3}{2}}_{(1,0)}(3))\}^2;$$

$$|T|^2 = (2\pi)^9 \cdot \gamma^{-9/2} \cdot |T_N|^2; \quad \gamma = \frac{m}{\hbar^2}$$

$$|T|^2 = |T_{\text{sing; } S=\frac{1}{2}}|^2 + |T_{\text{trip; } S=\frac{1}{2}}|^2 + |T_{\text{trip; } S=\frac{3}{2}}|^2$$

Here sing and trip refer to the spin in the first pair.

Finally the correlation cross section is

$$\frac{d^3\sigma}{d\Omega_1 d\Omega_2 dE_1} = \gamma^{\frac{2\pi}{\hbar\omega_{in}}} \cdot 10.0 \cdot \mathcal{S} \cdot |T|^2$$

where $\mathcal{S}$ is the phase space factor

Now partial wave decomposition of $T^S_{(S_i,T_i)}(\vec{q}_i)$ gives

$$T^S_{(S_i T_i)}(\vec{q}_i) = \sum_\ell \frac{2\ell+1}{2} \cdot T^S_{\ell(S_i,T_i)}(q_i) P_\ell(\cos\theta)$$

where θ_i is the production angle of subsystem i relative the direction of the deuteron in the total center-of-mass.

Each $T^{S}_{\ell(S_i,T_i)}$ is evaluated from an integral equation of one continuous variable q and the amplitude is parameterized with six parameters (a_i)

$$T^{S}_{\ell(S_i T_i)} = \frac{a_1 + a_2 q + a_3 q^2}{1 + a_4 q + a_5 q^2 + a_6 q^3} \cdot Q_\ell(s,q) \cdot (s-q^2)^{\frac{1}{2}}$$

where Q_ℓ is a LeGendre function of the second kind and s is square of the energy in the total center-of-mass system. This is done by the code EBEN-HOEH1. For a chosen laboratory energy of the incident proton the program produces 24 parameters a_i (i = 1,6) corresponding to

$$\ell = 0,5 \text{ and } S = \tfrac{3}{2}\ (\sigma^{np} = 1);\ S = \frac{1}{2}\ (\sigma^{np} = 0,1 \text{ and } \sigma^{pp} = 1)$$

This code takes about 20 minutes to run on the Uppsala IBM 370/155 computer.

These amplitudes are used as inputs in a second code (EBENHOEH2) which calculates the correlation cross section for a chosen kinematical situation. The only necessary modification was a change of the subroutine calculating the kinematics in order to make the program calculate noncoplanar correlations.

3.5 INTERPRETATION OF THE BREAKUP AMPLITUDE

The structure of the integral equations for the breakup amplitudes indicates that the breakup process can be looked upon as a two-step process, involving first rearrangement scattering (or production) and then final pair breakup (Fig 3). The Faddeev component with the smallest relative momentum is the most important one. However, Amado[4] showed that only the sum of all three Faddeev components gives a peak with a shape close to the Migdal-Watson shape. Indeed, Ebenhöh[17] later demonstrated that the predicted shapes from the SPM-model and Migdal-Watson model of an n-d breakup experiment at T_n = 18.4 MeV only differed slightly provided the same n-n scattering lengths were used.

The second characteristic feature of breakup spectra is the peak corresponding to low spectator energy. Ebenhöh explained this peak as due to a peaking in one of the rearrangement amplitudes. These off-shell amplitudes are backward peaked in terms of the pair-production angle as defined in section 3.4.

4. RESULTS AND CONCLUSIONS

The present comparisons with SPM calculations cover the following coplanar spectra measured at Uppsala

1. Symmetric spectra ($\theta_3 = \theta_4 = 20^\circ$, 25°, 35° and 40°)
   Asymmetric spectra ($\theta_4 = 20^\circ$, 25°, 35°, 40°, 45°, 50° and 55°; $\theta_3 = 30^\circ$)
   These spectra were obtained with rather poor statistics and have been reported[11].
2. Symmetric spectra ($\theta_3 = \theta_4 = 30.0^\circ$; 36.7°)
   Asymmetric spectra ($\theta_4 = 43.4^\circ$, 75.4° and $\theta_3 = 30.0^\circ$)
   These spectra were obtained with better statistical accuracy and have not been reported before.

All these spectra are shown in Fig 4-18 together with the SPM calculations. Throughout this work no adjustment in absolute magnitude of either experimental data or theory has been made unless explicitly specified. The agreement is very good in most cases. However, there are certain systematic deviations. For low relative energy of the two protons in the final state the difference in absolute magnitude is worse. However, for large relative energies, i.e. large opening angle between the detectors, the agreement in absolute magnitude is good over the whole spectrum. It should be noted that the shifts in the asymmetric spectra between the MSIA (modified simple impulse approximation) fits and the experimental distributions reported in ref 11 is reproduced by the SPM calculations. In Fig 10 an MSIA fit to data between the arrows is given for comparison (dashed line).

In Figs 19-27 the noncoplanar data from ref 13 are compared with the SPM calculations. The agreement or disagreement is almost the same all over the range of angles between the scattering planes. This is clearly shown in Fig 28 where the theoretical and experimental peak cross sections are compared. The dashed line is a least square fit of a renormalized SPM distribution ($N = 0.86$). As expected from the analysis of the coplanar spectra, the agreement in absolute magnitude at the maximum of the peak is worse for the largest angles between the scattering planes where the relative pp energy is smaller than for the coplanar spectrum. As pointed out in ref 13 the peak for large angles between the scattering planes cannot be explained by a peaking in the production amplitude for a pp pair[17].

A closer look at the different amplitudes contributing in the SPM shows that it is the amplitude corresponding to final state interaction in the pp pair which causes the peaking for large angles between the scattering planes.

In Fig 29 a comparison between data obtained at Rice University at T_p = 12.5 MeV[15] for pp and pn coplanar symmetric correlations of the d(p,2p)n reaction and SPM predictions is made. The experimental peak cross sections of ref 15 corresponding to minimum neutron energy are compared with the corresponding SPM values. Where there was no peak in either the theoretical or experimental distribution the cross section corresponding to minimum neutron energy was taken. It should be kept in mind that the Rice correlation cross sections were measured relative the elastic pd data of A C Wilson et al[20] and are probably some percent to small[21] also at 12.5 MeV. From this comparison, one infers that in the pn case the agreement is quite good over the whole angular region but in the pp case the same trend which could be observed in the comparison with the Uppsala symmetric coplanar data at T_p = 10.0 MeV is found also here. The disagreement is worse for small opening angles between the detectors, i.e. at low pp relative energy in the final state at the point corresponding to minimum neutron energy where the comparison is made. The experimental points corresponding to the smallest opening angle (30°) are probably wrong. The excellent agreement for the rest of the pn distribution makes it unlikely that this point should disagree so drastically and because of the monitor method used (the spectra were accumulated simultaneously) the corresponding pp value is probably also wrong.

There is also a "micro" structure in the experimental distributions which might be due the cross section normalization procedure used. One of the coincidence detectors was used as monitor detector. There is an appreciable background in the single spectra at the position corresponding to protons elastically scattered from deuterium at small scattering angles. This is due to the fast rising $p\text{-}C^{12}$ elastic cross section for small scattering angles. This might also be the reason for the strange experimental values for $\theta_3 + \theta_4 = 30.0^\circ$.

The neglect of Coulomb forces in the calculations should give deviations between the SPM calculations and the experimental data. Most of the data used in the comparisons were taken to enhance the "quasifree" pp mechanism.

The experimental peak corresponding to minimum neutron energy is according to Ebenhöh[17] due to a peaking in the off-shell rearrangement amplitude in the same kinematic region. Consequently no direct relationship between the pp force used and the calculated peak cross sections can be expected. Nevertheless, an attempt to make a rough estimate of the influence of Coulomb forces was made in the following way. Fig 30 shows the pp cross section, calculated with the effective range formalism without Coulomb forces, used in the SPM calculation (dashed line) and the s-wave pp cross section ($\theta_{pp}^{cm} = 90^{\circ}$) with Coulomb forces included[29] (solid line). The experimental points were taken from refs 27 and 28. As can be seen the pp cross section used in the SPM calculations is smaller than the actual values above ~ 3.3 MeV proton energy. Using the effective range formalism without Coulomb forces the effective range parameters (a_{pp} and r_o) were changed so that the cross sections calculated matched the 90° center-of-mass pp cross section at 3.0 and 7.0 MeV proton energy. The result was the dashed and dotted line in Fig 30 ($a_{pp} = 6.37$ fm and $r_o = 1.37$ fm). These parameters were then used for the pp force in the SPM calculations. The results are shown in Figs 4, 6 and 9 as dashed lines.

The agreement is worse except for the spectrum corresponding to $\theta_3 = \theta_4 = 20.0^{\circ}$ ($\varphi_3 = 0^{\circ}$ and $\varphi_4 = 180^{\circ}$)(Fig 4). This last change might be related to the fact that for lower energies the pp cross section calculated with the "new" effective range parameters is smaller than the cross section calculated with the old parameters. This rough way of introducing Coulomb effects would indicate that the inclusion of Coulomb forces makes the disagreement worse between experiment and theory. However, due to the simplicity of the approach, it might be an example of what Lovelace[3] has expressed "The three-body system is far too treacherous to be delt with by physical intuition". It illustrates anyhow the importance of including Coulomb forces in a correct way in the SPM calculations. This is unavoidable if any reliable a test of the dynamical three-nucleon calculations is to be made. The neutron induced breakup reaction is not very useful for this purpose becasuse the nn scattering length is not well known and the experiments are extremely difficult to make with sufficient accuracy. It will take some time before a calculation including Coulomb forces, hard core effects, tensor forces and higher partial waves in the nucleon-nucleon interactions used will be performed. A detailed experimental investigation of polarization effects in the d(p,2p)n reaction might give information of the importance of the last two effects.

REFERENCES

1. L O Faddeev, Soviet Phys JETP 12 (1961) 1014
2. A N Mitra and V S Bashin, Phys Rev 131 (1963) 1265
3. C Lovelace, Phys Rev 135 (1964) B 1225
4. R Amado, Phys Rev 132 (1963) 485
   R Aaron and R D Amado, Phys Rev 150 (1966) 857
5. A E Everett, Phys Rev 126 (1962) 831
6. A F Kuckes, R Wilson and P F Cooper Am Phys 15 (1961) 193
7. A H Cromer, Phys Rev 129 (1963) 1680
   A H Cromer and E H Thorndike, Phys Rev 131 (1963) 1680
   C N Brown and E H Thorndike, Phys Rev 177 (1969) 2067
8. K M Watson, Phys Rev 88 (1952) 1163
   A B Migdal, Soviet Phys JETP 1 (1955) 2
9. V Valković, D Rendić, V A Otte, W von Witsch and G C Phillips, Nucl Phys A 166 (1971) 547
10. R D Amado, Three-Body Problem in Nuclear and Particle Physics, North Holland Publ Co (1970) p 40
11. B Sundqvist, A Johansson, L Amtén, L Gönczi, I Koersner and B Palmgren, Tandem Laboratory Report, Uppsala 1972, TLU 4/72
12. B Sundqvist, A Johansson, L Amtén, L Gönczi and I Koersner, Tandem Laboratory Report, Uppsala 1973, TLU 11/73
13. B Sundqvist, A Johansson, L Gönczi and I Koersner, Tandem Laboratory Report, Uppsala 1973, TLU 10/73
14. B Sundqvist and A Johansson, Tandem Laboratory Report, Uppsala 1973, TLU 12/73
15. E Andrade, V Valković, D Rendic and G C Phillips, Nucl Phys A 183 (1972) 145
16. R T Cahill and I H Sloan, Nucl Phys A 165 (1971) 161
17. W Ebenhöh, Nucl Phys A 191 (1972) 97
18. H Klein, Dissertation der Universität zur Köln, 1972
19. J P Burq, J C Cabrillat, M Chemarin, B Ille and G Nicolai, Nucl Phys A 179 (1972) 371

20. A S Wilson, M C Taylor, I C Legg and G C Phillips, Nucl Phys A 130 (1969) 624

21. B Sundqvist, A Johansson and L Glantz
TLU 14/73, Tandem Laboratory Report, Uppsala 1973

22. Advances in Nuclear Physics, eds M Baranger and E Vogt, I Duck Vol I (Plenum Press, New York, 1968) pp 343-410

23. E O Alt, P Grassberger and W Sandhas, Nucl Phys B2 (1967) 167

24. H Ekstein, Phys Rev 101 (1956) 880

25. R D Amado, Three-Body Problem in Nuclear and Particle Physics, North Holland Publ Co (1970) pp 243-262

26. Y Yamaguchi, Phys Rev 95 (1954) 1628

27. D J Knecht, P F Dahl and S Messelt, Phys Rev 148 (1966) 1031

28. E J Zimmerman, R O Kerman, S Singer, P G Kruger and W Jentschke Phys Rev 96 (1954) 1322

29. A Johansson, B Sundqvist, L Gönczi and I Koersner
TLU 3/72, Tandem Labaoratory Report, Uppsala 1972

FIGURE CAPTIONS

Fig 1 The rotating target holder used in the experiment.

Fig 2 Two-particle scattering with a third particle passing unaffected.
a. with an arbitrary amplitude.
b. with a separable amplitude.

Fig 3 Diagramatic visualization of the last-pair interaction model.

Figs 4-9 Coplanar symmetric correlation spectra for T_p = 10.0 MeV and the corresponding SPM distributions (solid line). The dashed lines in Figs 4, 6 and 9 correspond to SPM with a modified pp interaction.

Figs 10-18 Coplanar asymmetric correlation spectra for T_p = 10.0 MeV and the corresponding SPM distributions (solid line).

Figs 19-27 Noncoplanar symmetric correlation spectra for T_p = 10.0 MeV and the corresponding SPM distributions (solid line).

Fig 28 Experimental peak cross sections for noncoplanar correlations together with a curve calculated with the SPM code (solid line) and the latter distribution renormalized with a factor 0.86 (dashed line) as a function of the angle between the scattering planes. The normalization constant was determined by a least-squares procedure.

Fig 29 Experimental peak cross sections for coplanar symmetric pp and pn correlations at 12.5 MeV (Rice data) as a function of the polar angle of one of the detectors. The solid line is the SPM code pp distribution and the dashed one is the corresponding curve for pn correlations.

Fig 30 The center-of-mass pp cross section. The solid line is the s-wave pp cross section ($\theta_{cm}^{pp} = 90^{o}$) with Coulomb forces included. The dashed line the pp cross section calculated with the effective range formalism without Coulomb forces (a_{pp} = -7.76 fm ; r_o = 2.86 fm) and used in the SPM calculations. The dashed and dotted line is the corresponding cross section for (a_{pp} = -6.37 fm ; r_o = 1.37 fm). The experimental points are taken from refs 27 and 28.

Table I Effective range parameters used in the calculations

Nucleon pair	Spin	Isospin	Scattering length (fm)	Effective range (fm)
np	0	1	-23.68	2.67
pp	0	1	- 7.76	2.86
np	1	0	5.416	1.75

Table II Summery of cutoff radii extracted from the Uppsala measurement of the d(p,2p)n cross-section for T_p = 10.0 MeV; $\theta_3 = \theta_4$ = 30.0°; φ_3 = 0.0° and φ_4 = 180°

Month - Year	Extracted cut-off radius (fm)	Remarks
Jan -72	5.32 ± 0.06	Coplanar correlations [11]
April -72	5.63 ± 0.08	Noncoplanar correlations [13]
Sept -72	5.57 ± 0.05	Excitation function [14]
Dec -72	5.54 ± 0.06	Check of absolute scale
Jan -73	5.52 ± 0.05	Excitation function [14]
Weighted mean value	5.51 ± 0.03	

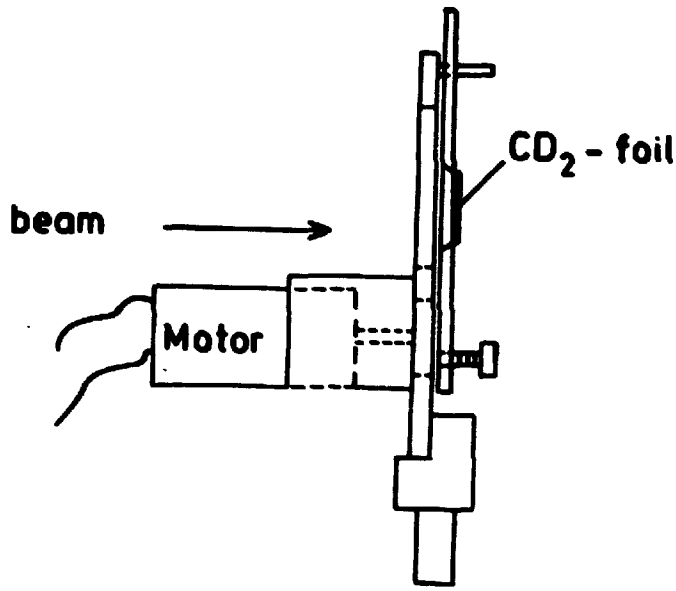

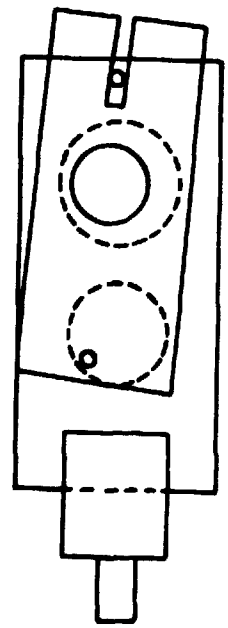

Fig 1

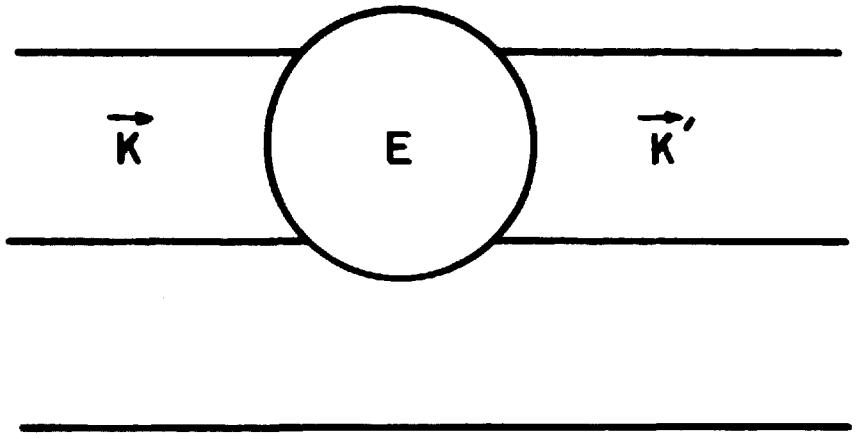

a

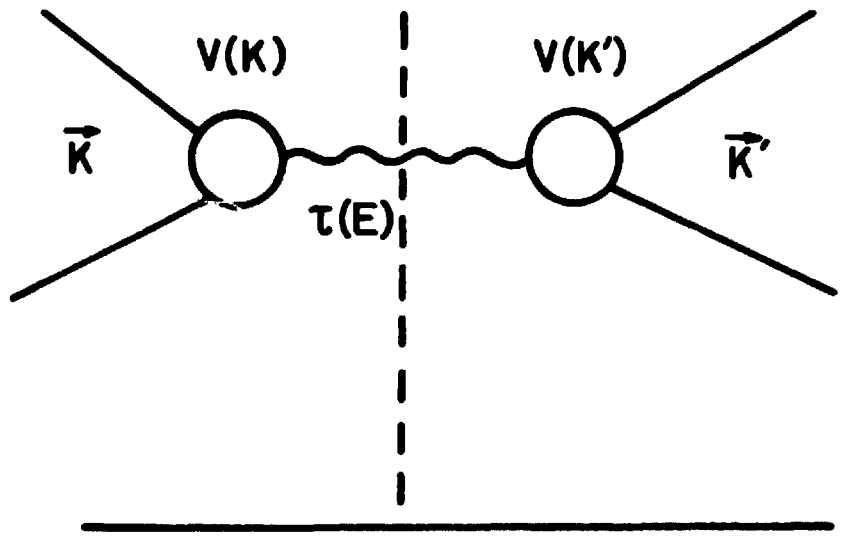

b

Fig 2

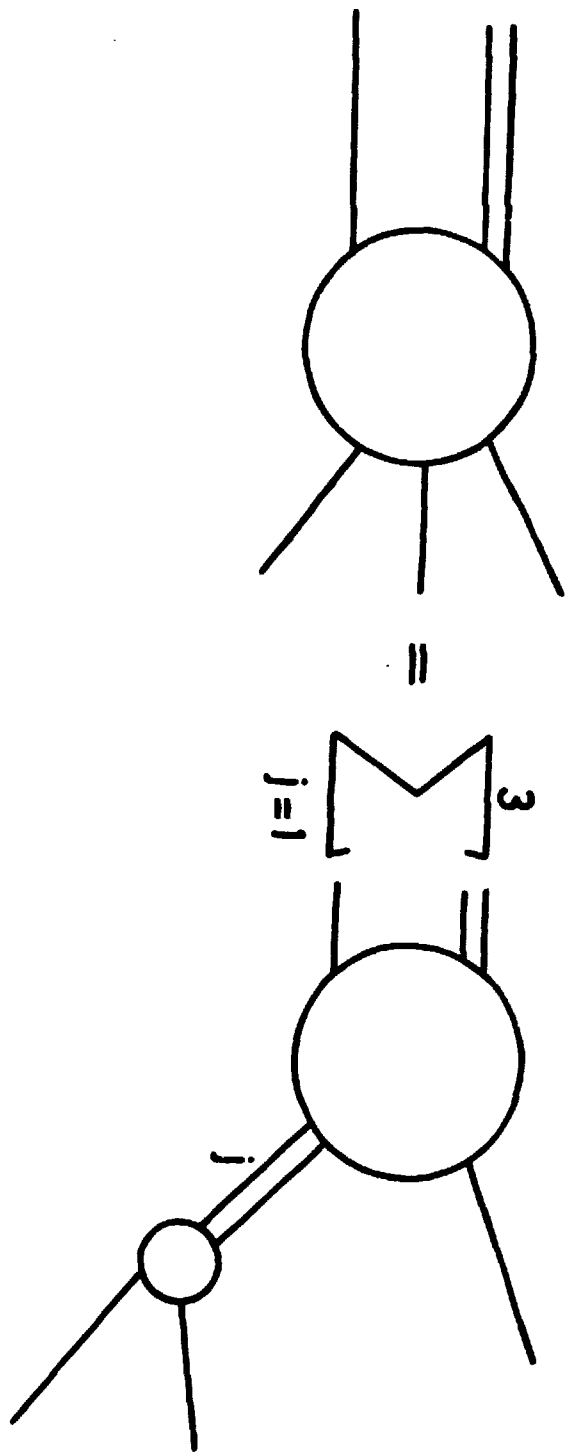

Fig 3

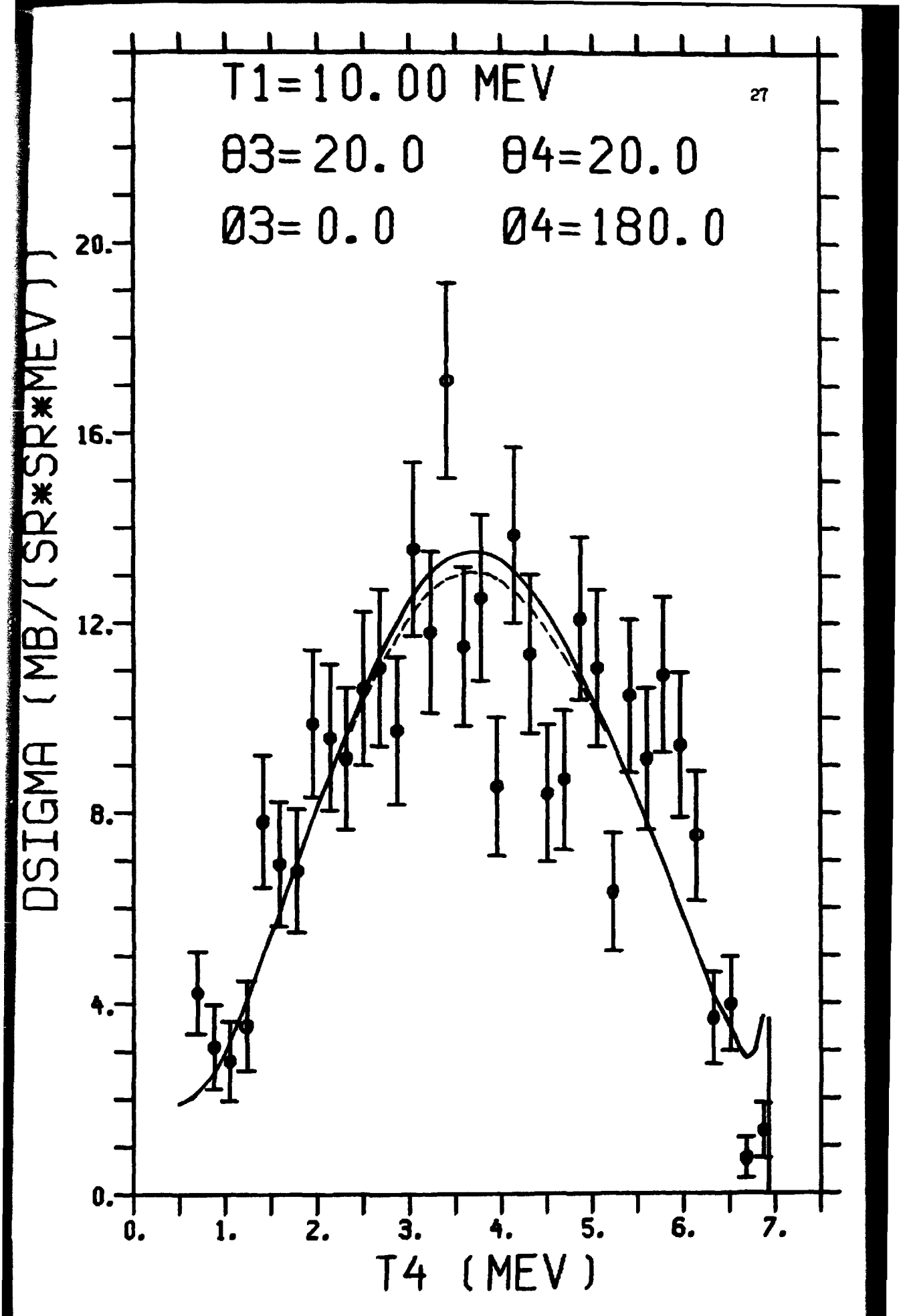
T1=10.00 MEV
θ3=20.0 θ4=20.0
Ø3= 0.0 Ø4=180.0
DSIGMA (MB/(SR*SR*MEV))
20.
16.
12.
8.
4.
0.
0. 1. 2. 3. 4. 5. 6. 7.
T4 (MEV)

Fig 4

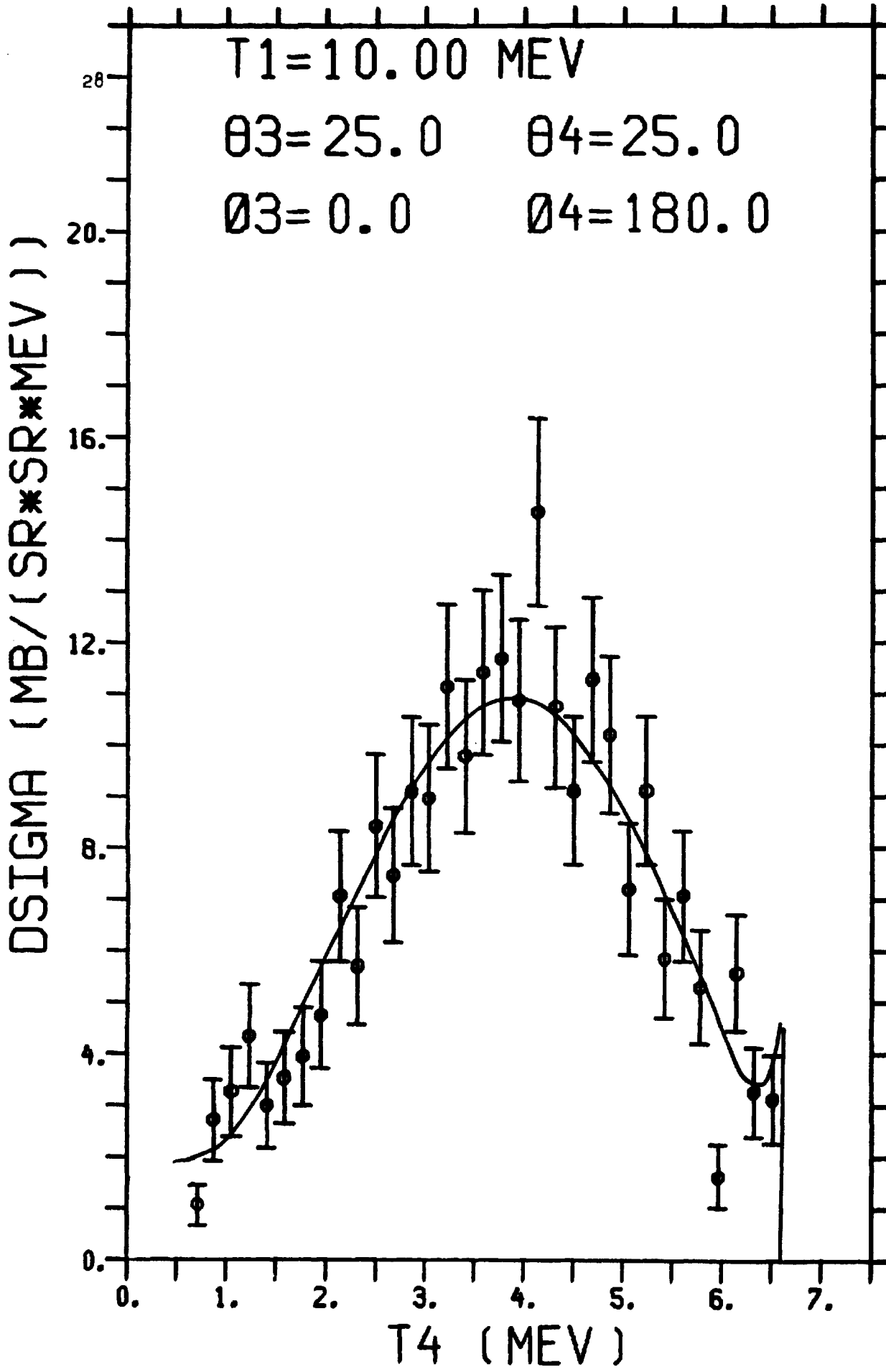
T1=10.00 MEV
θ3=25.0 θ4=25.0
Ø3= 0.0 Ø4=180.0
DSIGMA (MB/(SR*SR*MEV))
T4 (MEV)
0.
4.
8.
12.
16.
20.
28
0.
1.
2.
3.
4.
5.
6.
7.

Fig 5

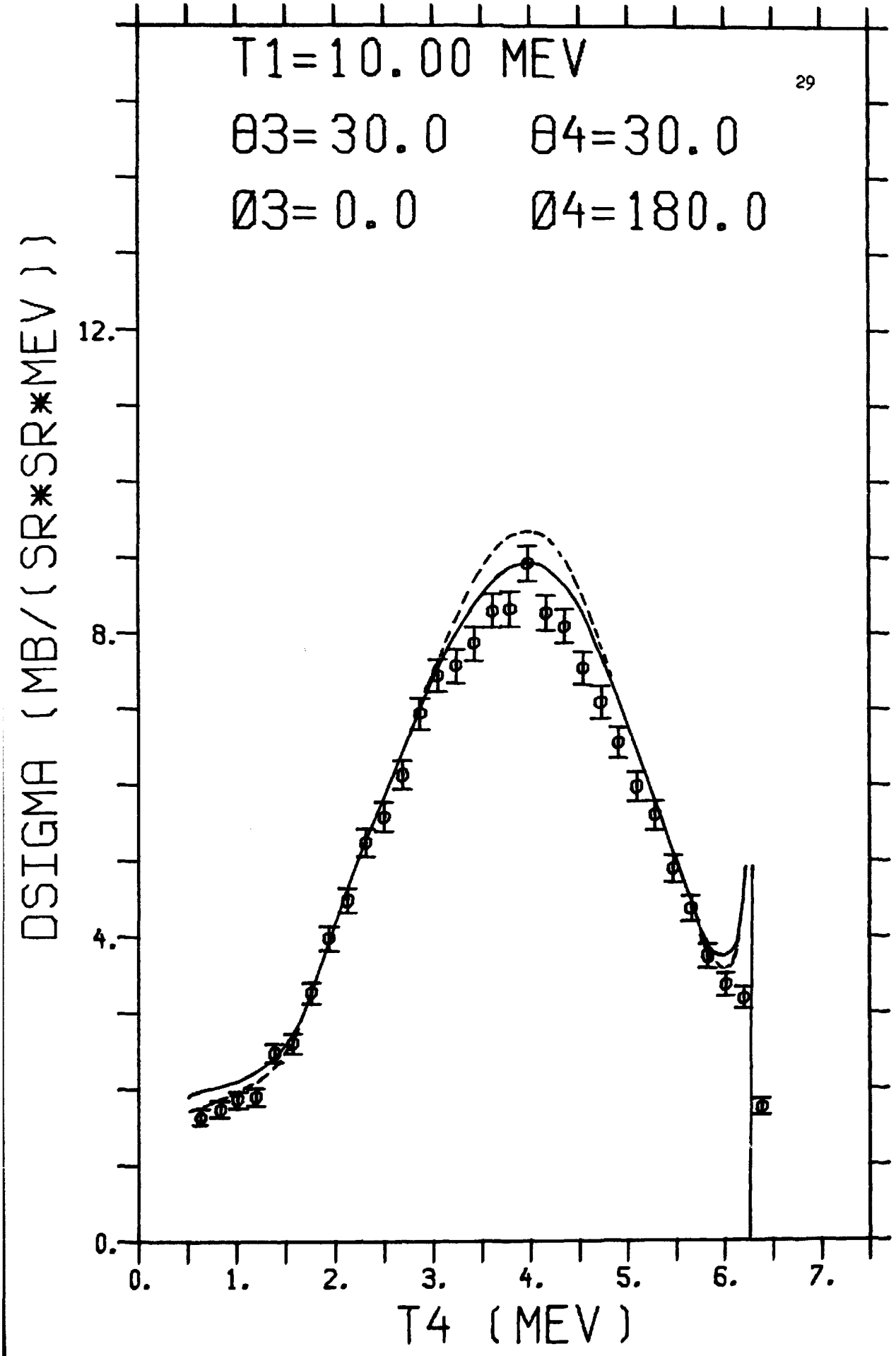
T1=10.00 MEV
θ3=30.0 θ4=30.0
Ø3= 0.0 Ø4=180.0
DSIGMA (MB/(SR*SR*MEV))
12.
8.
4.
0.
0. 1. 2. 3. 4. 5. 6. 7.
T4 (MEV)

Fig 6

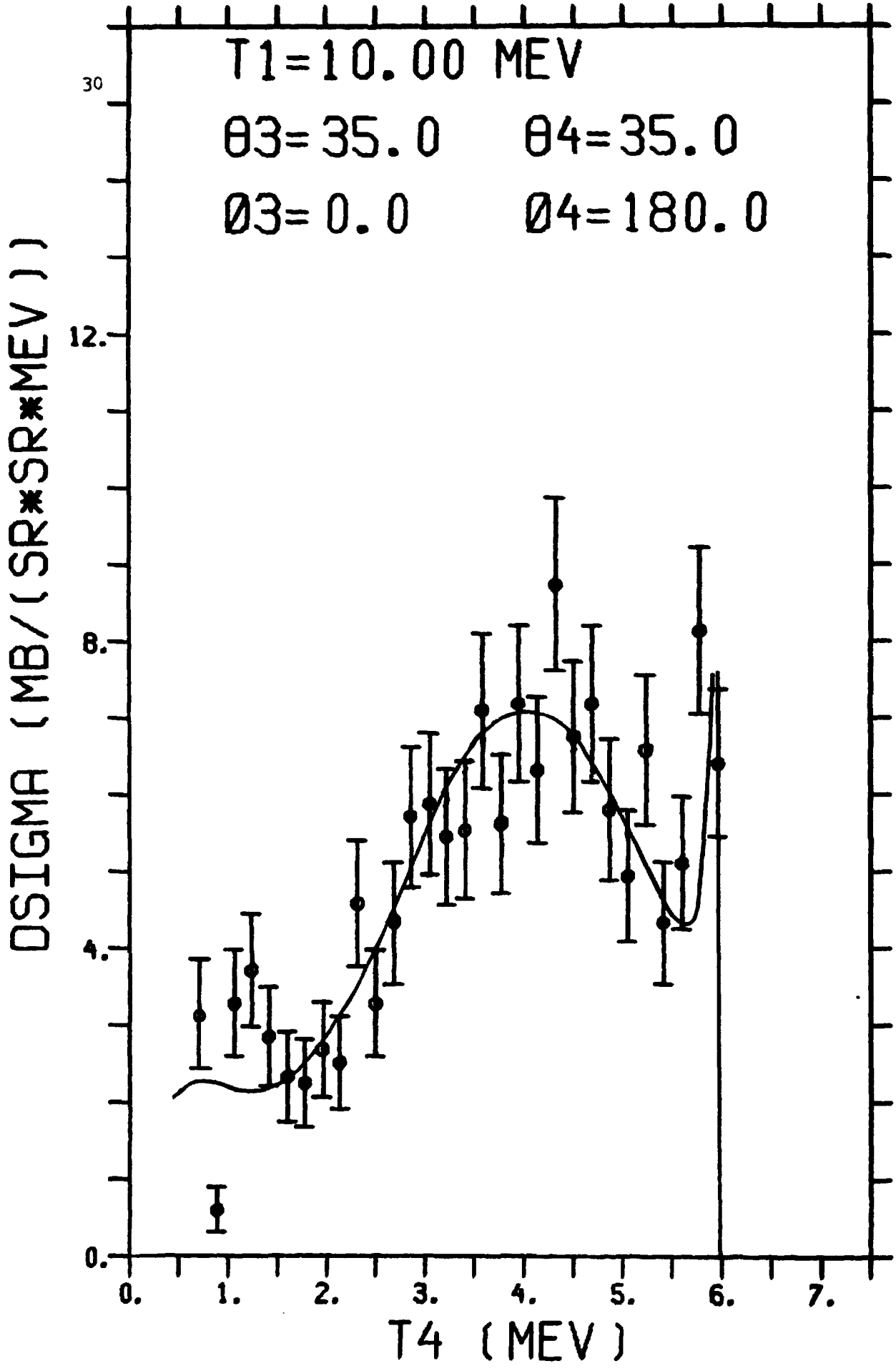
T1=10.00 MEV
θ3=35.0 θ4=35.0
Ø3=0.0 Ø4=180.0
DSIGMA (MB/(SR*SR*MEV))
30
12.
8.
4.
0.
0. 1. 2. 3. 4. 5. 6. 7.
T4 (MEV)

Fig 7

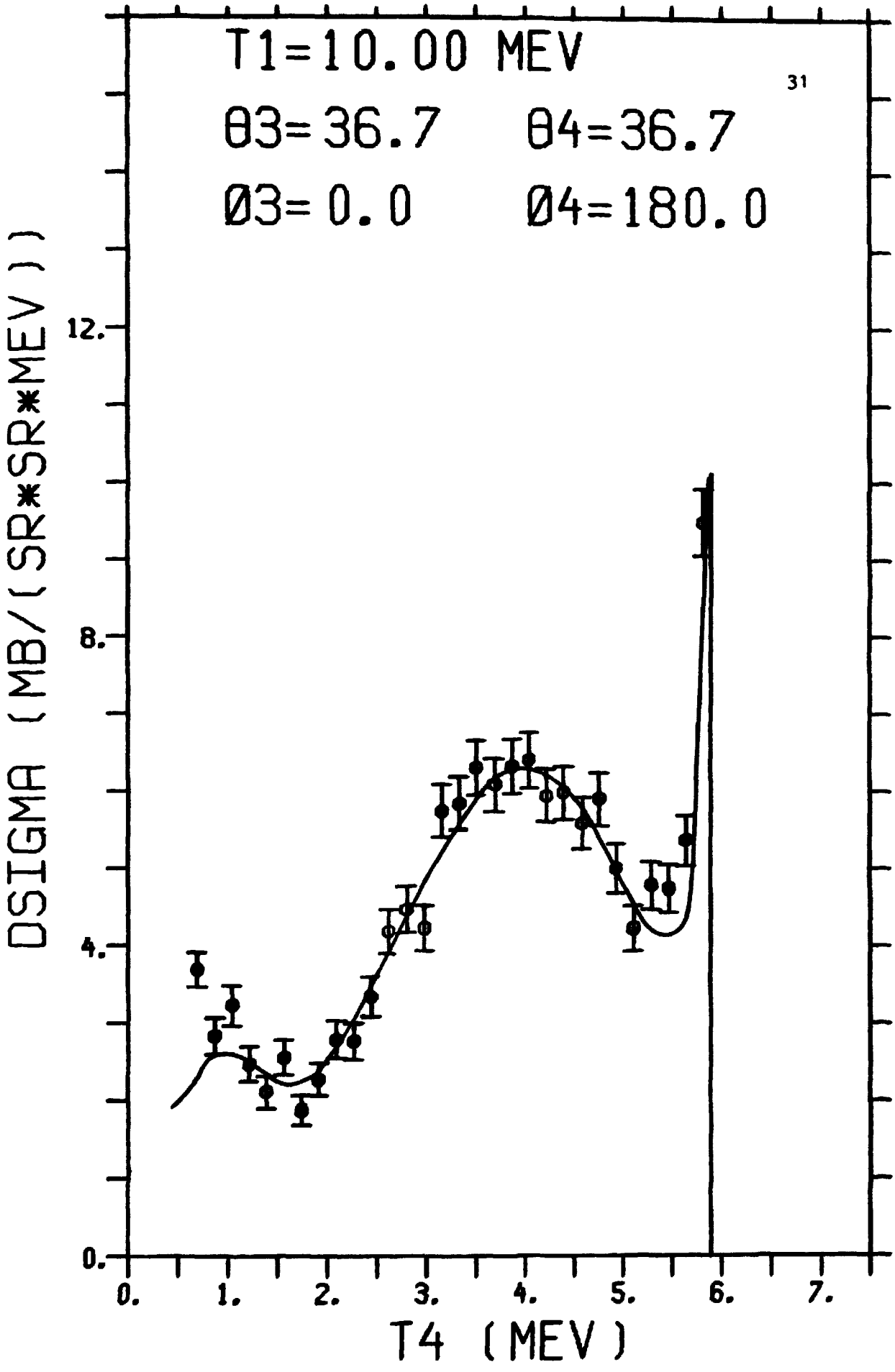
T1=10.00 MEV
θ3=36.7 θ4=36.7
Ø3= 0.0 Ø4=180.0
DSIGMA (MB/(SR*SR*MEV))
12.
8.
4.
0.
0. 1. 2. 3. 4. 5. 6. 7.
T4 (MEV)

Fig 8

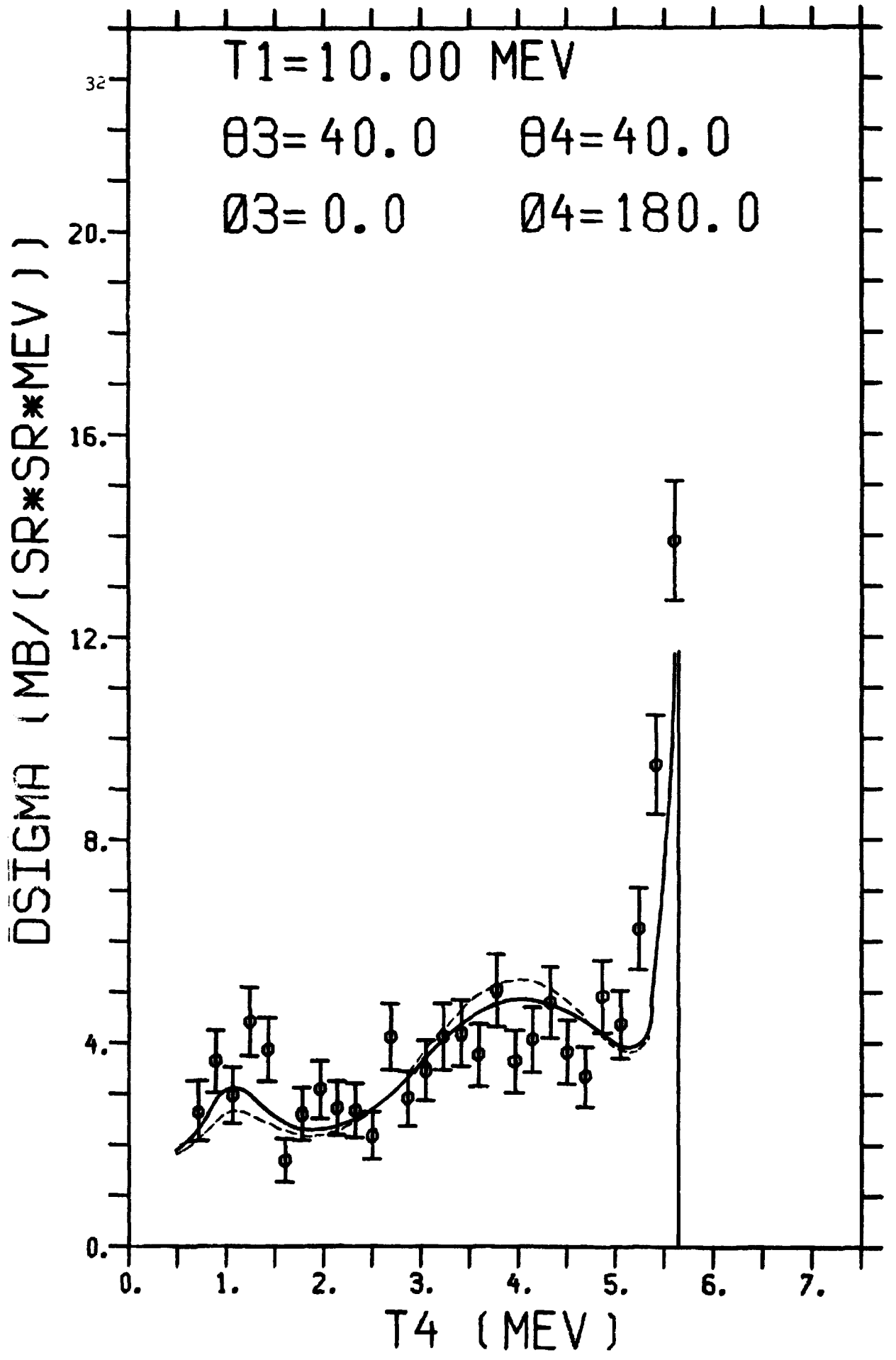
T1=10.00 MEV
θ3=40.0 θ4=40.0
Ø3= 0.0 Ø4=180.0
DSIGMA (MB/(SR*SR*MEV))
32
20.
16.
12.
8.
4.
0.
0. 1. 2. 3. 4. 5. 6. 7.
T4 (MEV)

Fig 9

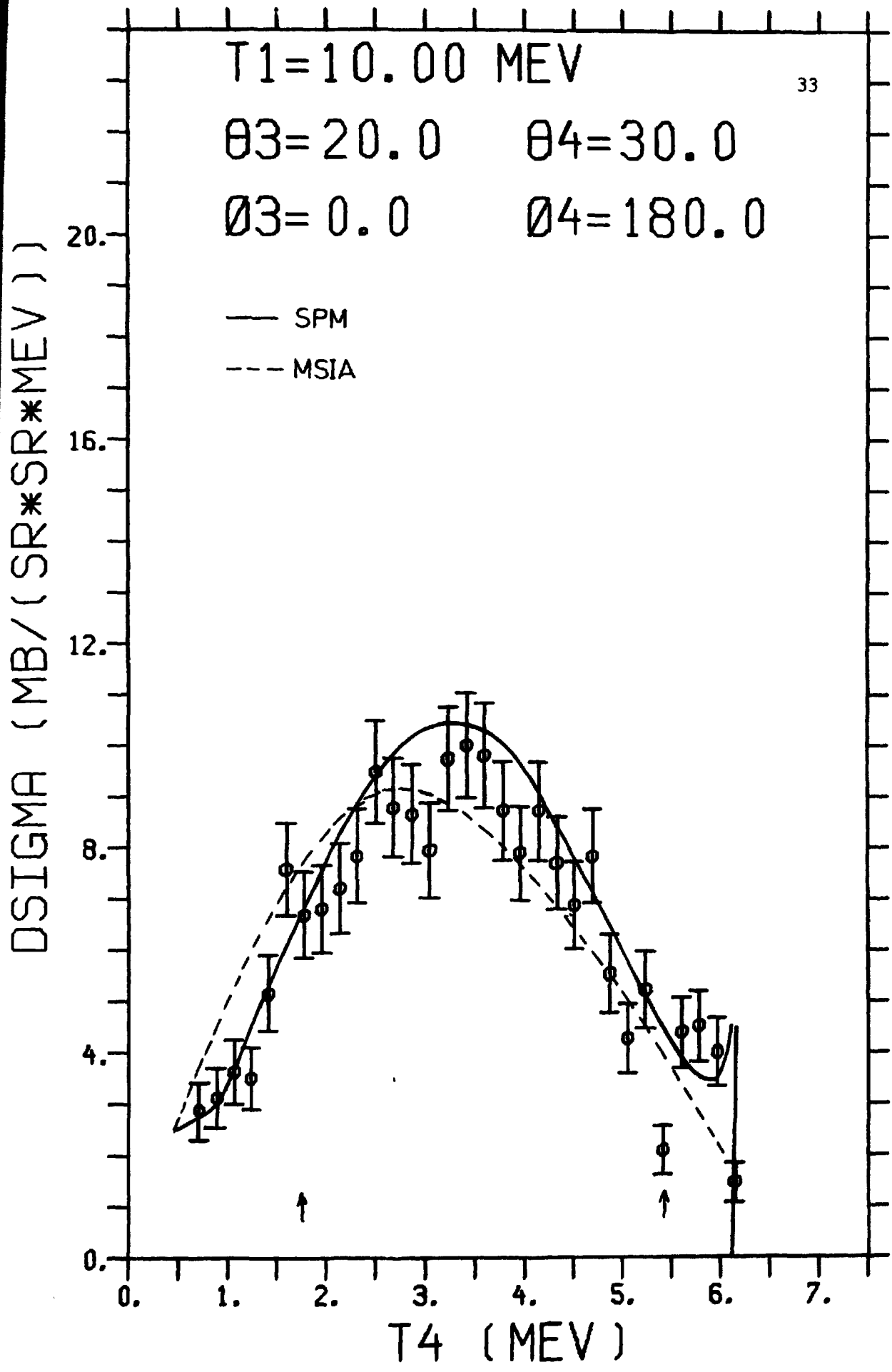
T1=10.00 MEV
θ3=20.0 θ4=30.0
Ø3= 0.0 Ø4=180.0
SPM
MSIA
DSIGMA (MB/(SR*SR*MEV))
0.
4.
8.
12.
16.
20.
0. 1. 2. 3. 4. 5. 6. 7.
T4 (MEV)

Fig 10

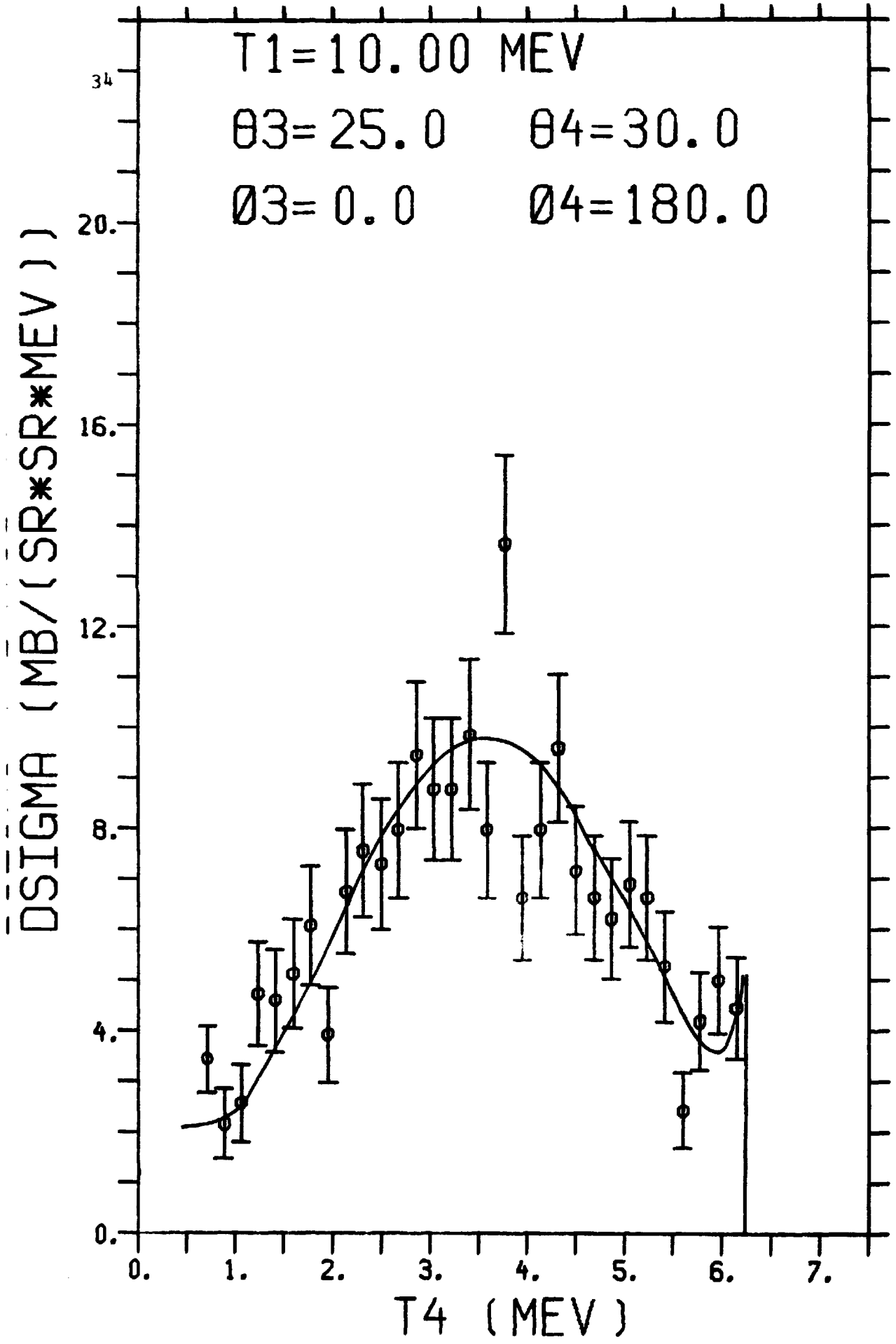
T1=10.00 MEV
θ3=25.0 θ4=30.0
Ø3=0.0 Ø4=180.0
DSIGMA (MB/(SR*SR*MEV))
T4 (MEV)
0.
4.
8.
12.
16.
20.
34
0.
1.
2.
3.
4.
5.
6.
7.

Fig 11

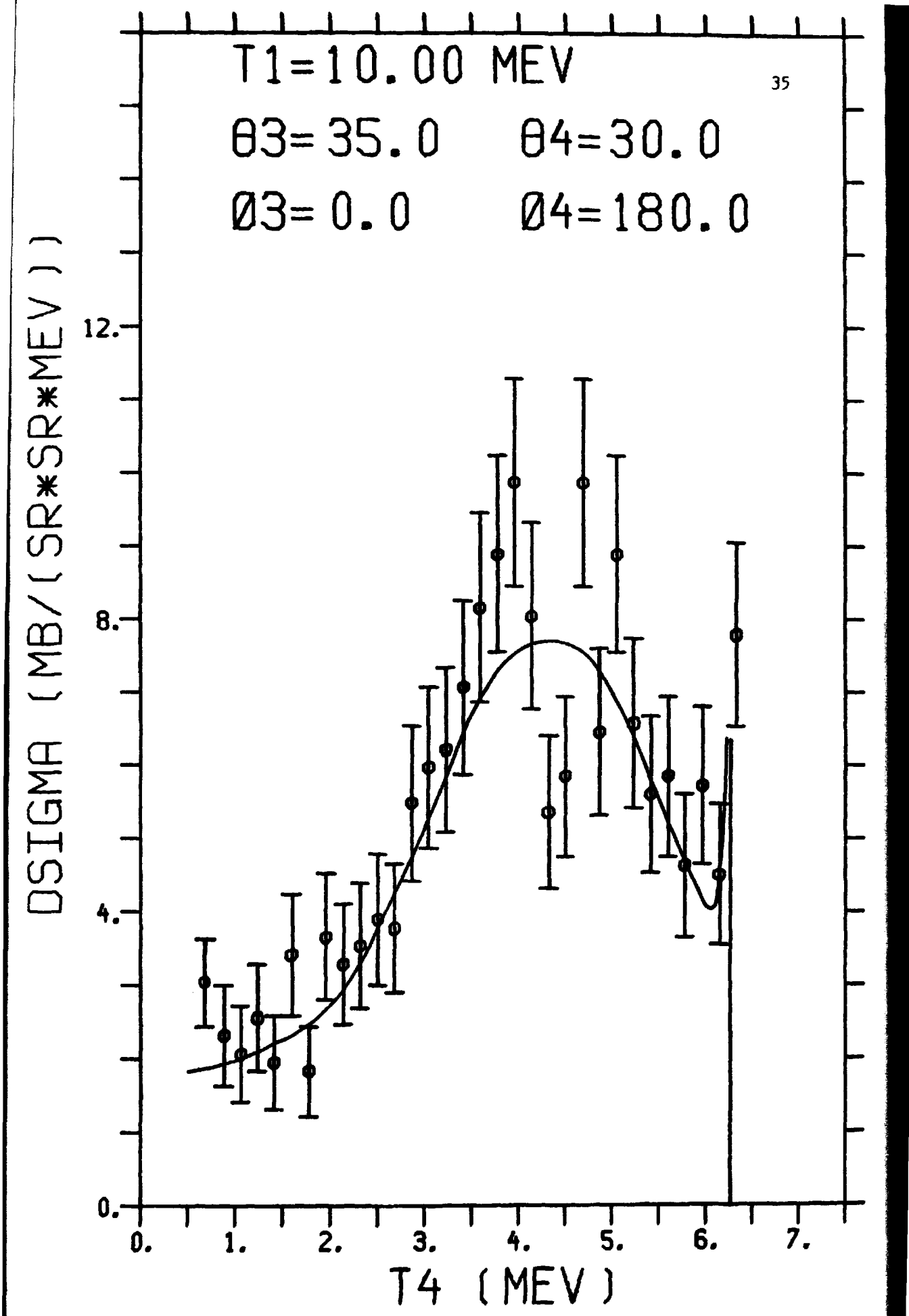
T1=10.00 MEV
θ3=35.0 θ4=30.0
Ø3=0.0 Ø4=180.0
DSIGMA (MB/(SR*SR*MEV))
12.
8.
4.
0.
0. 1. 2. 3. 4. 5. 6. 7.
T4 (MEV)

Fig 12

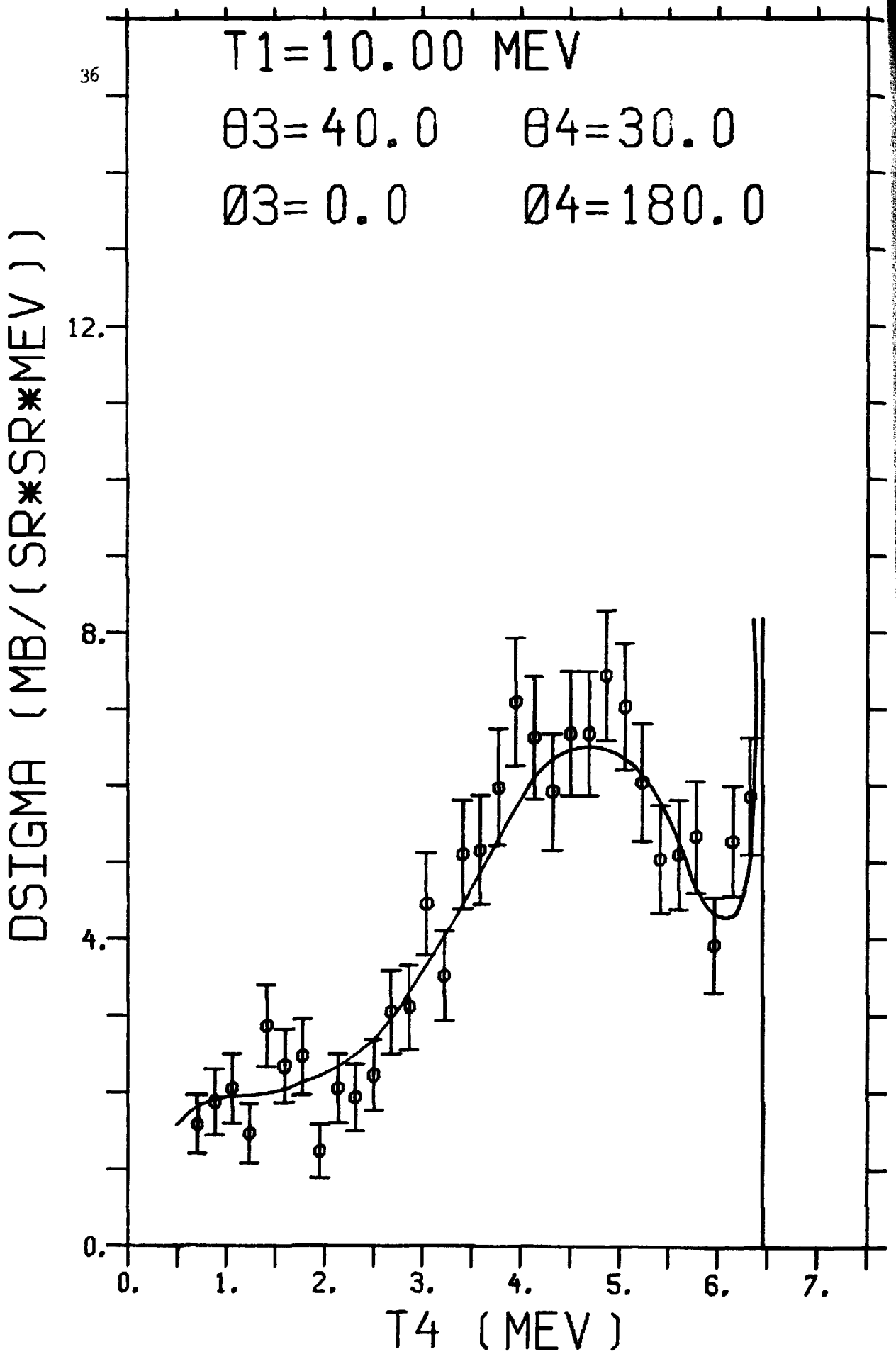
T1=10.00 MEV
θ3=40.0 θ4=30.0
Ø3=0.0 Ø4=180.0
DSIGMA (MB/(SR*SR*MEV))
0.
4.
8.
12.
0. 1. 2. 3. 4. 5. 6. 7.
T4 (MEV)

Fig 13

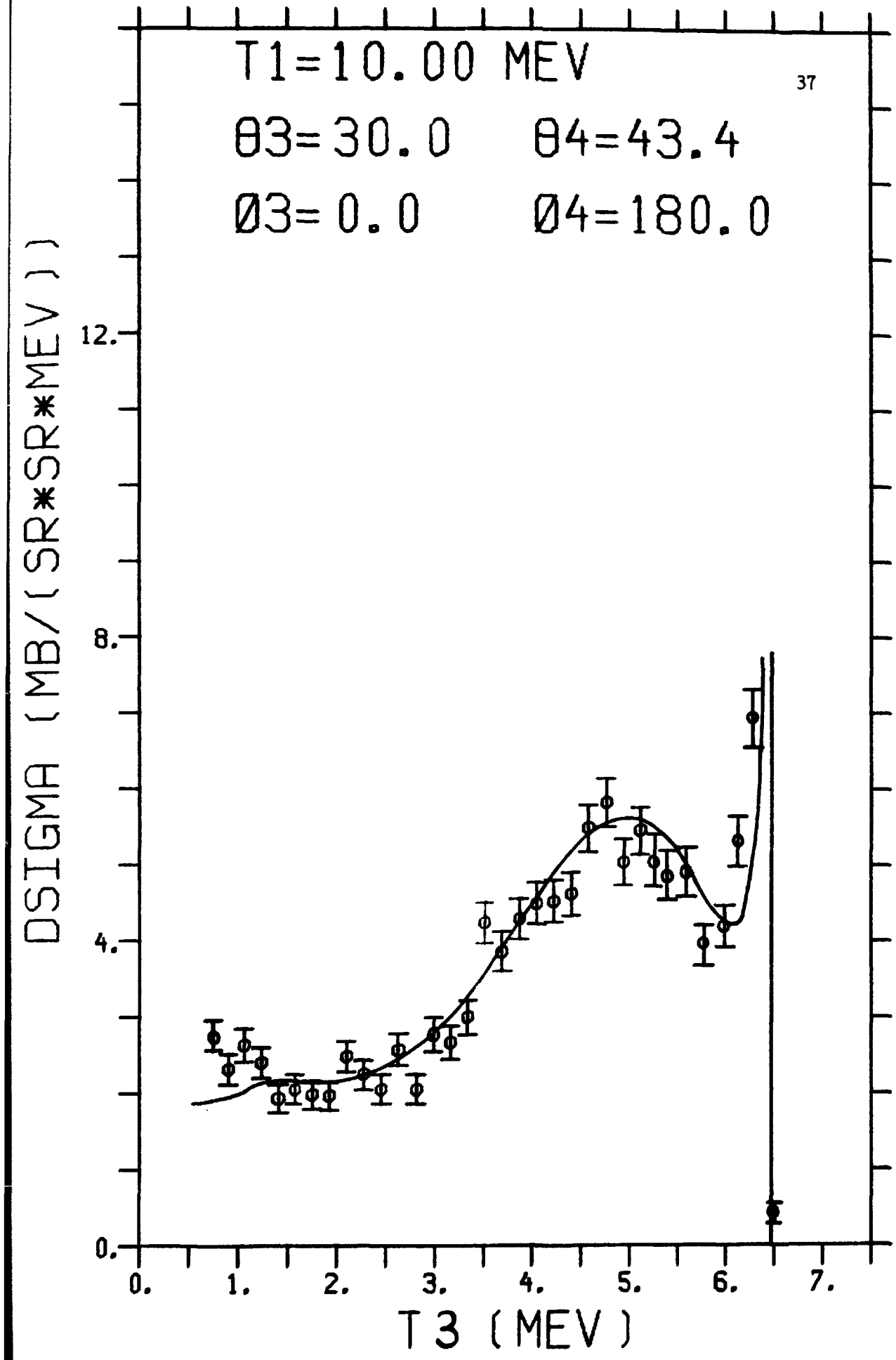
T1=10.00 MEV
θ3=30.0 θ4=43.4
Ø3=0.0 Ø4=180.0
DSIGMA (MB/(SR*SR*MEV))
12.
8.
4.
0.
0. 1. 2. 3. 4. 5. 6. 7.
T3 (MEV)

Fig 14

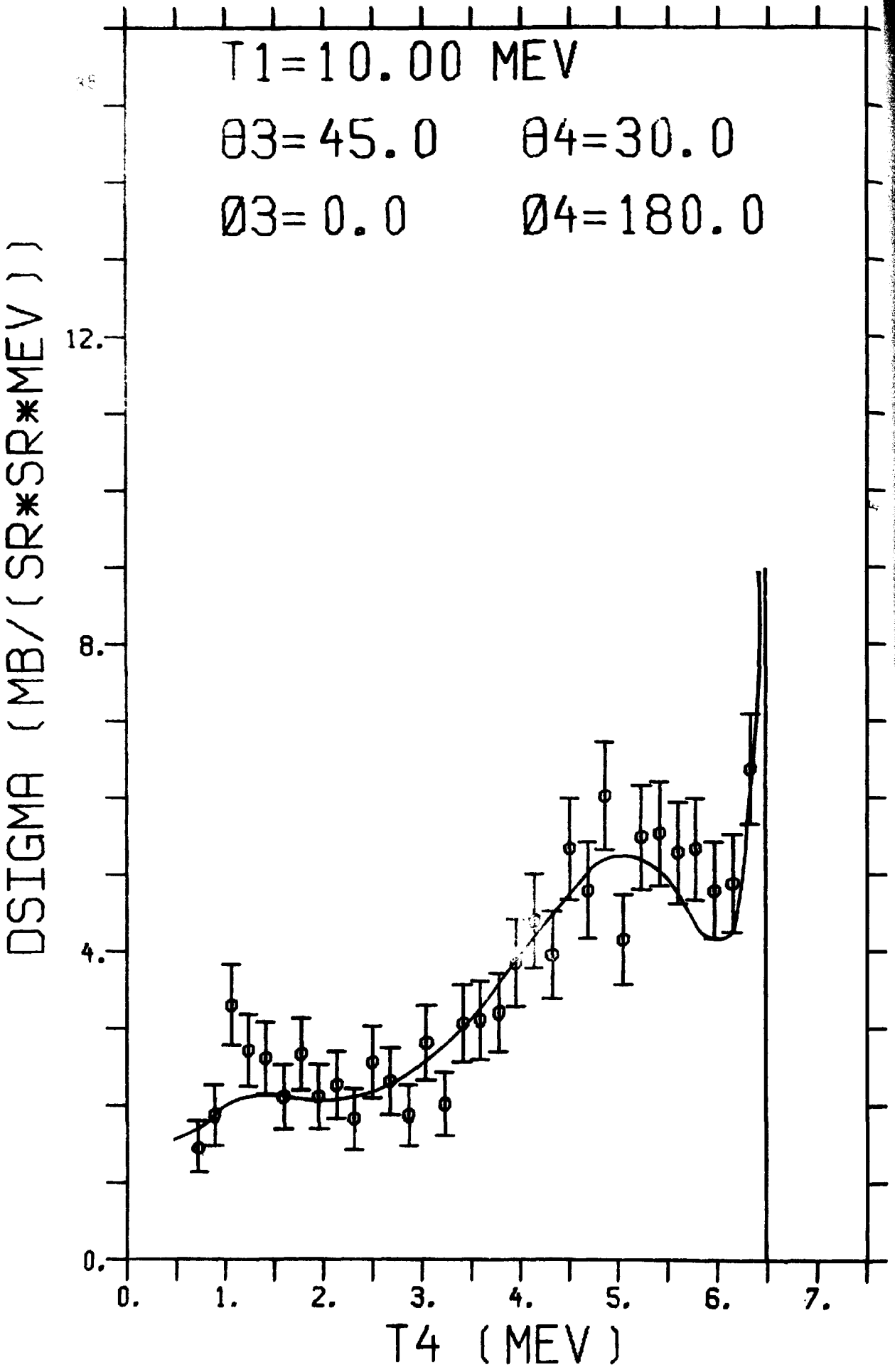
T1=10.00 MEV
θ3=45.0 θ4=30.0
Ø3=0.0 Ø4=180.0
DSIGMA (MB/(SR*SR*MEV))
0.
4.
8.
12.
0.
1.
2.
3.
4.
5.
6.
7.
T4 (MEV)

Fig 15

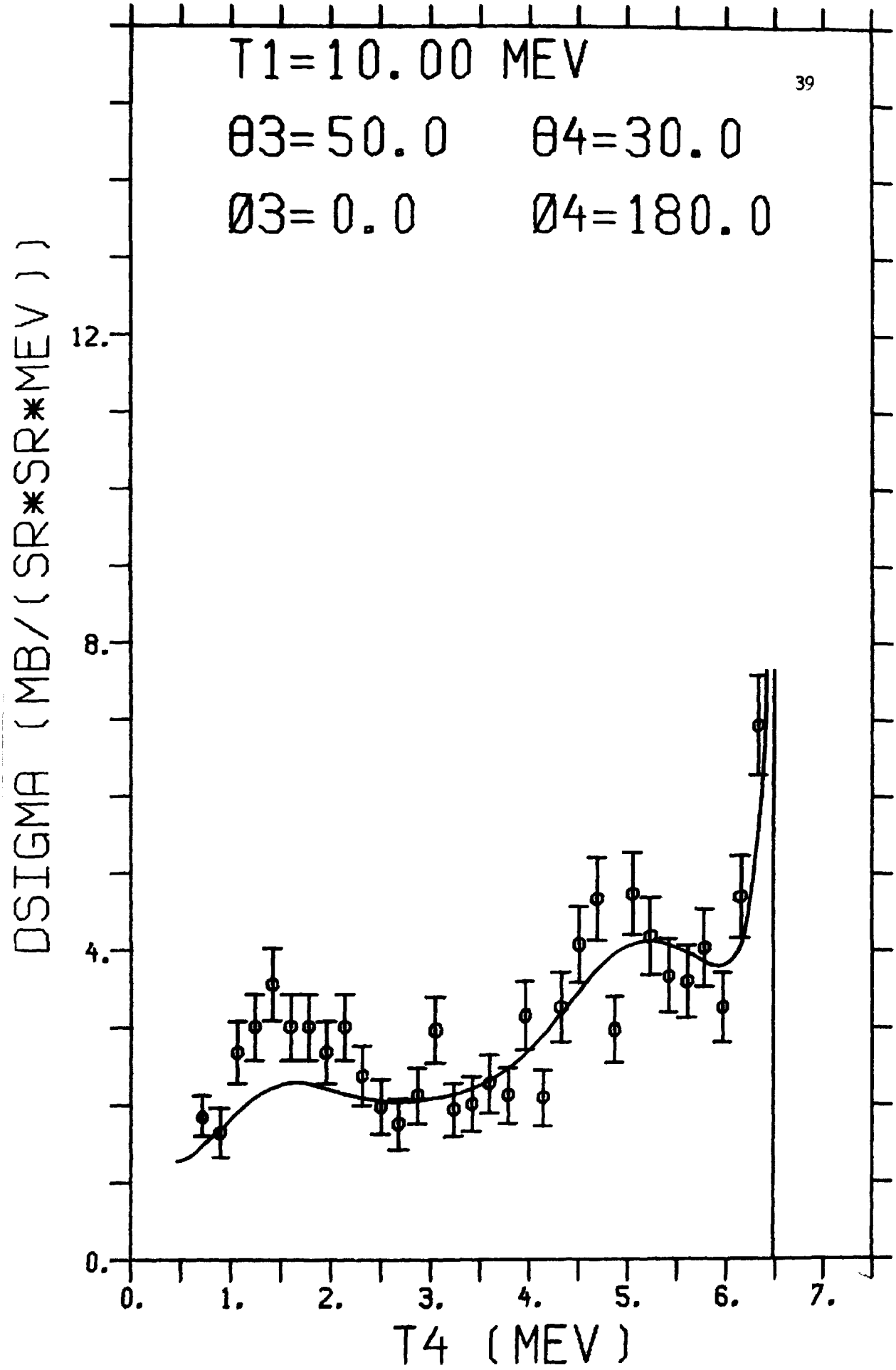
T1=10.00 MEV
39
θ3=50.0 θ4=30.0
Ø3=0.0 Ø4=180.0
DSIGMA (MB/(SR*SR*MEV))
12.
8.
4.
0.
0. 1. 2. 3. 4. 5. 6. 7.
T4 (MEV)

Fig 16

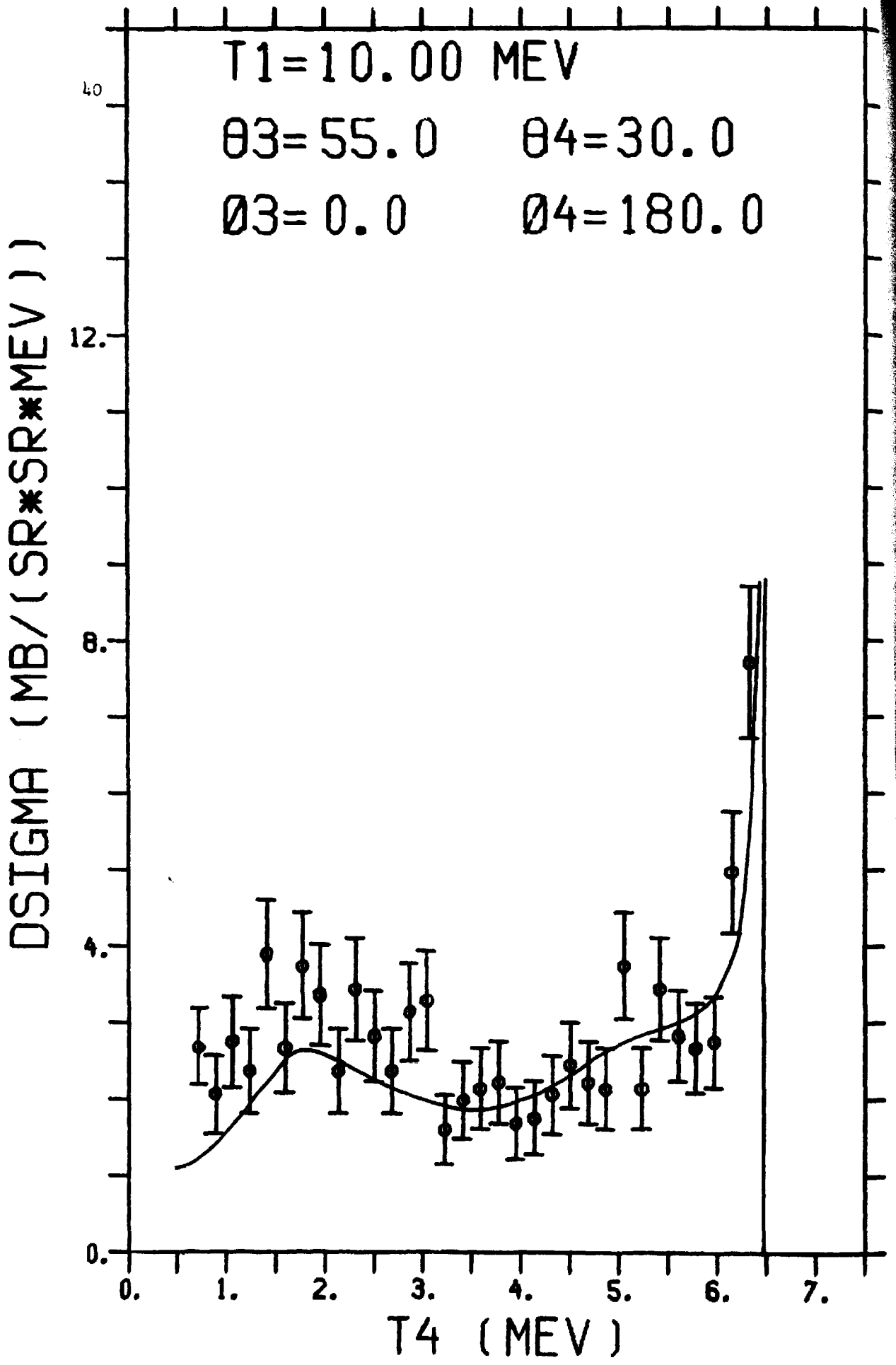
T1=10.00 MEV
θ3=55.0 θ4=30.0
Ø3= 0.0 Ø4=180.0
DSIGMA (MB/(SR*SR*MEV))
40
12.
8.
4.
0.
0. 1. 2. 3. 4. 5. 6. 7.
T4 (MEV)

Fig 17

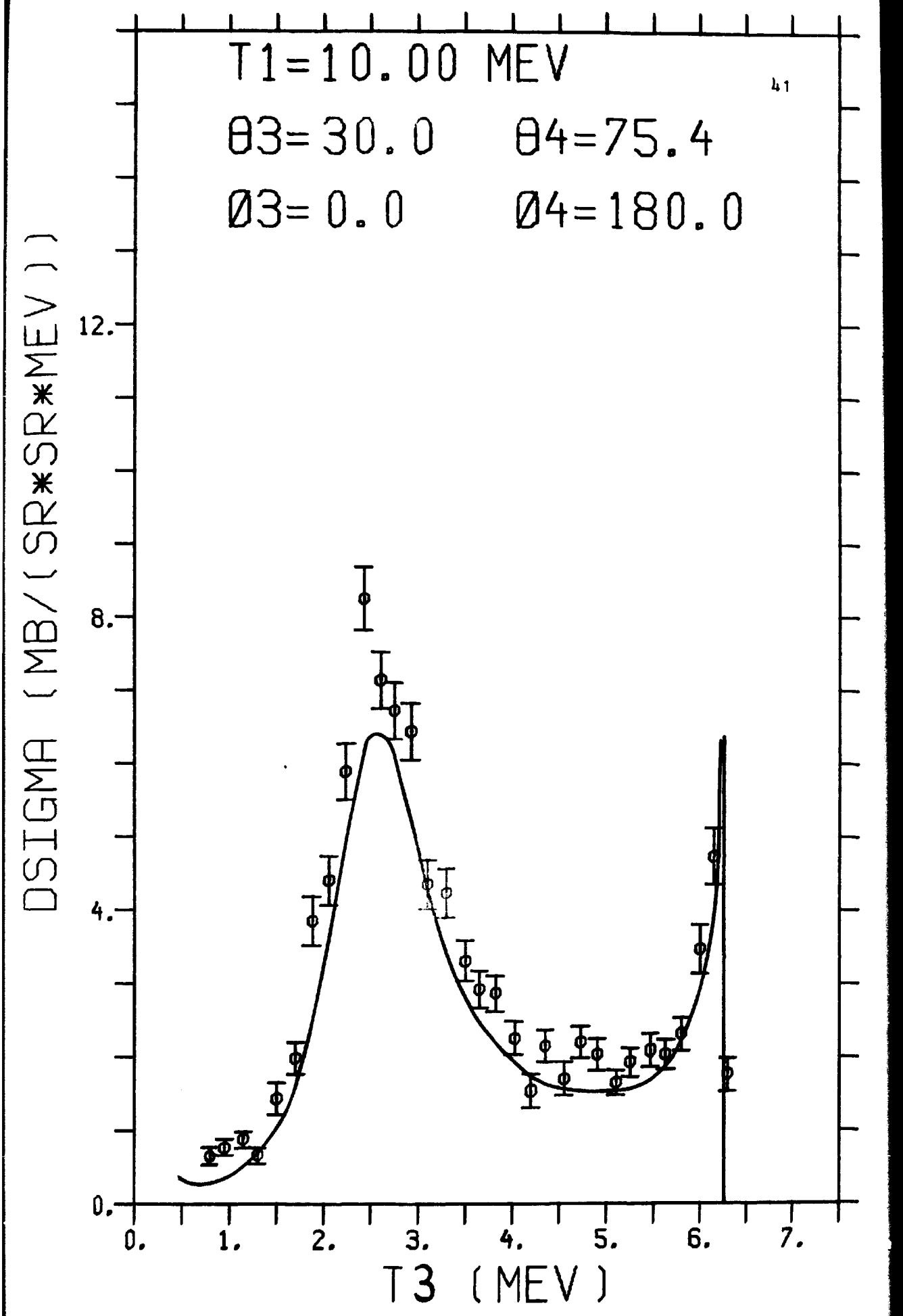
T1=10.00 MEV
41
θ3=30.0 θ4=75.4
Ø3=0.0 Ø4=180.0
DSIGMA (MB/(SR*SR*MEV))
12.
8.
4.
0.
0. 1. 2. 3. 4. 5. 6. 7.
T3 (MEV)

Fig 18

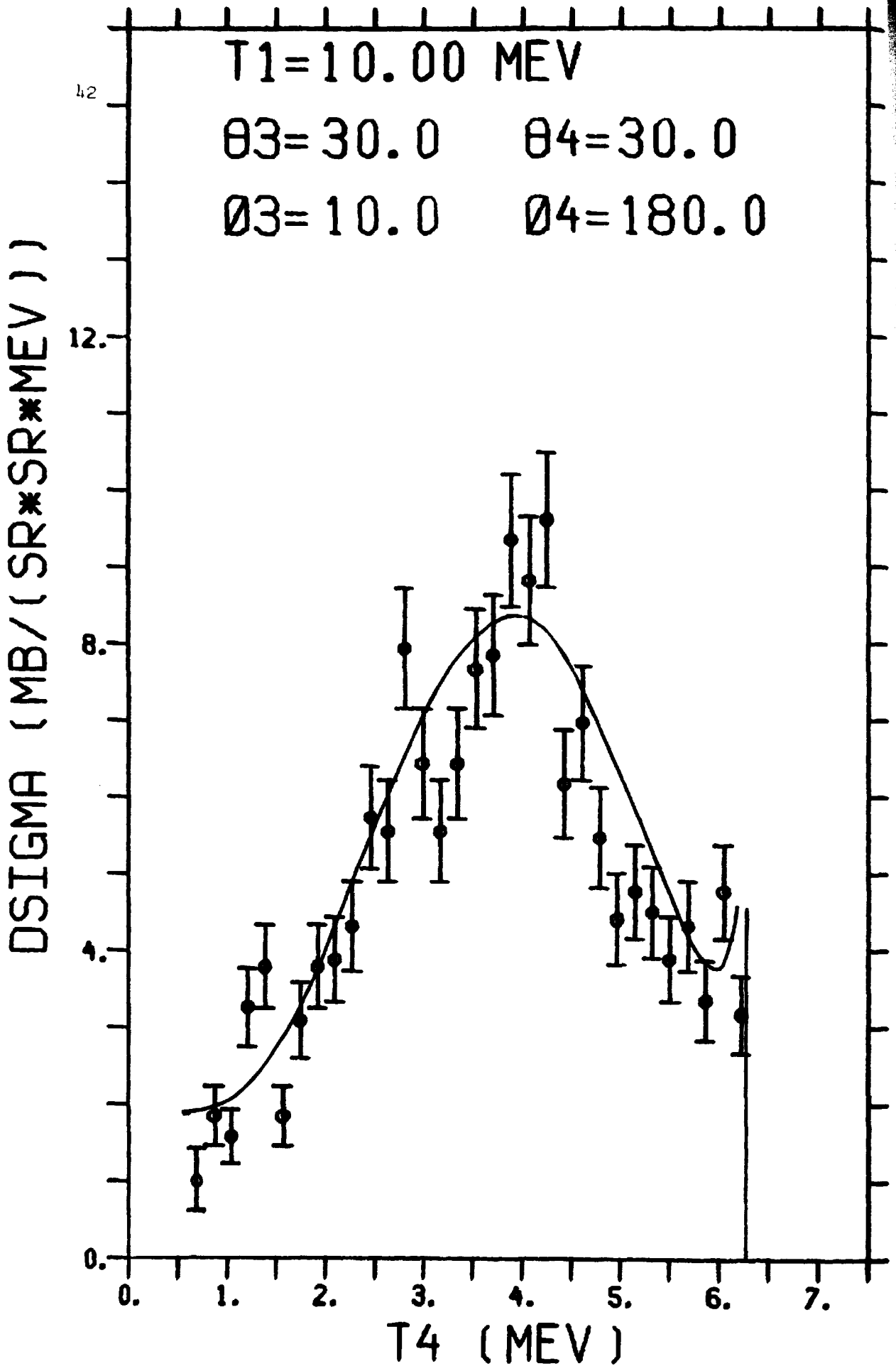
T1=10.00 MEV
θ3=30.0 θ4=30.0
Ø3=10.0 Ø4=180.0
DSIGMA (MB/(SR*SR*MEV))
0.
4.
8.
12.
0. 1. 2. 3. 4. 5. 6. 7.
T4 (MEV)

Fig 19

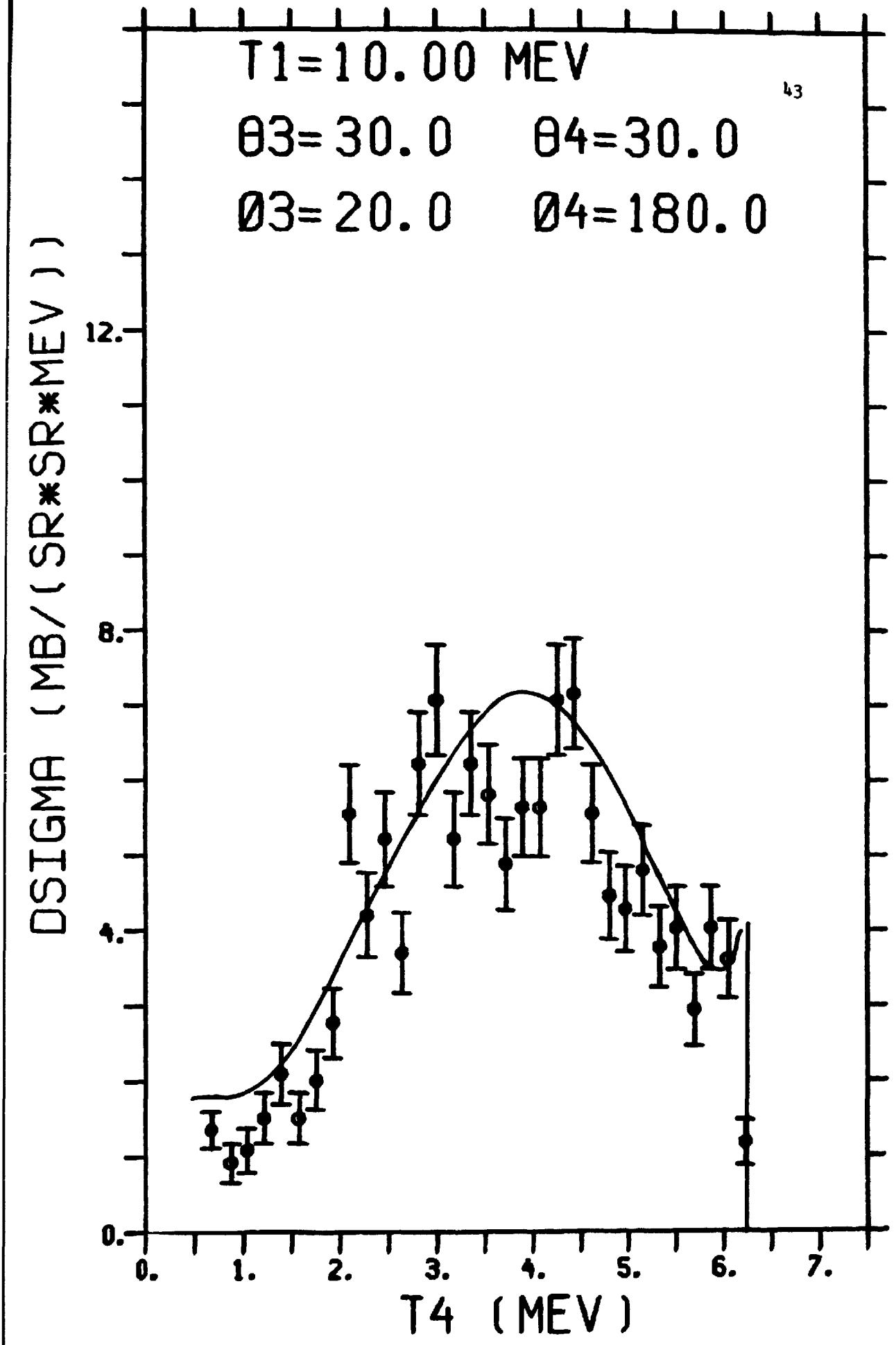
T1=10.00 MEV
θ3=30.0 θ4=30.0
Ø3=20.0 Ø4=180.0
DSIGMA (MB/(SR*SR*MEV))
12.
8.
4.
0.
0. 1. 2. 3. 4. 5. 6. 7.
T4 (MEV)

Fig 20

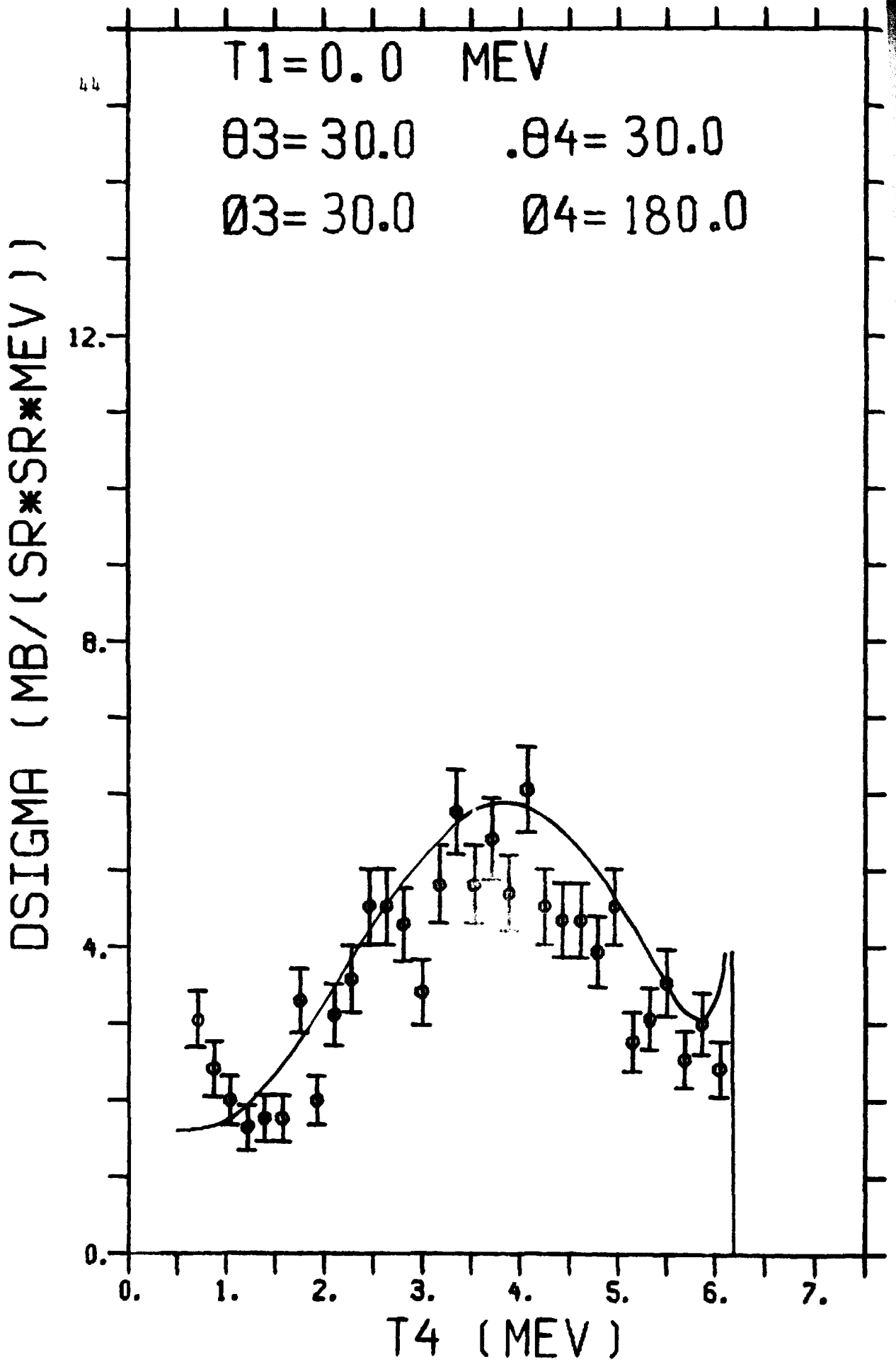
T1=0.0 MEV
θ3=30.0 θ4=30.0
Ø3=30.0 Ø4=180.0
DSIGMA (MB/(SR*SR*MEV))
0.
4.
8.
12.
0.
1.
2.
3.
4.
5.
6.
7.
T4 (MEV)

Fig 21

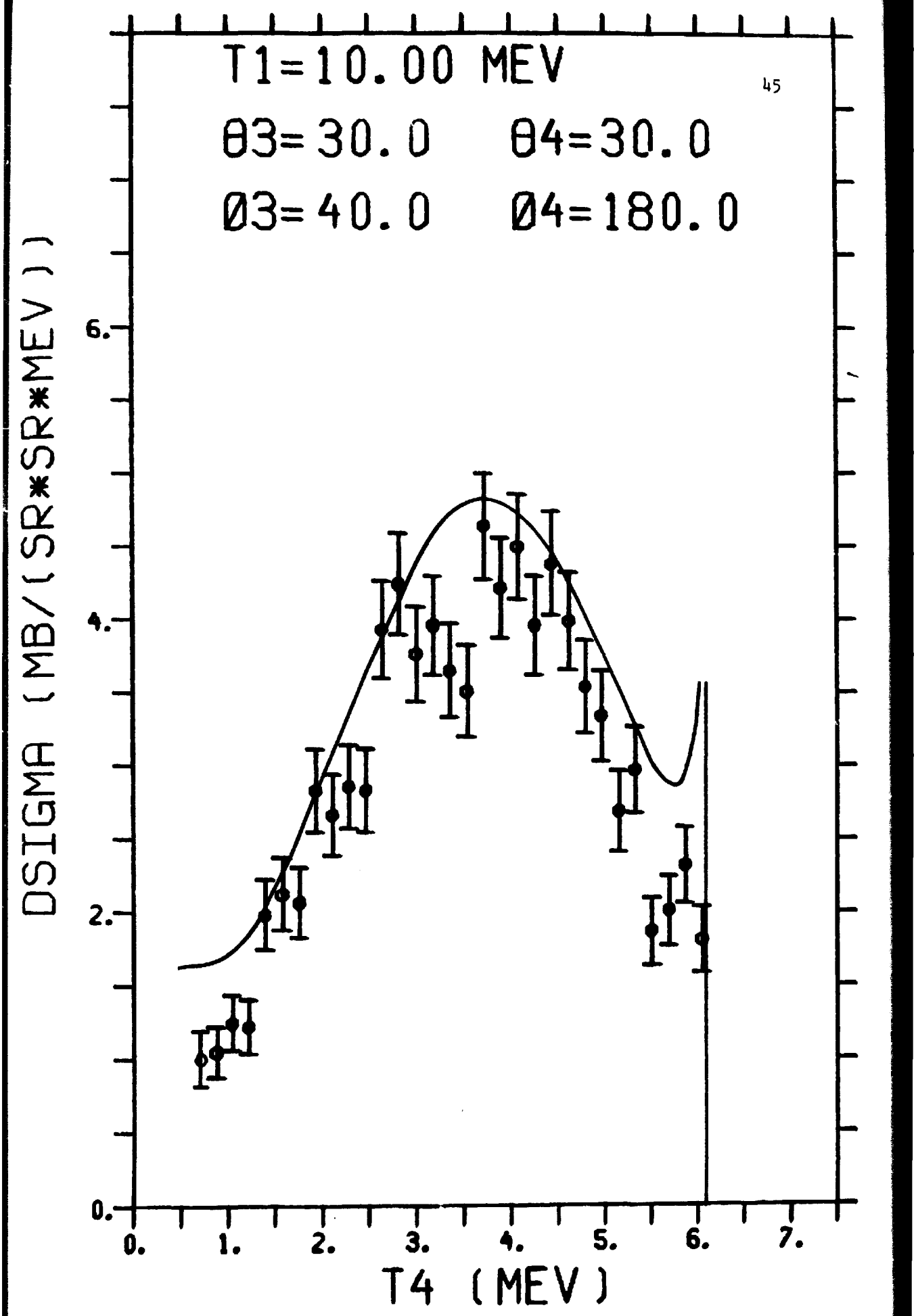
T1=10.00 MEV
θ3=30.0 θ4=30.0
Ø3=40.0 Ø4=180.0
DSIGMA (MB/(SR*SR*MEV))
0.
2.
4.
6.
0. 1. 2. 3. 4. 5. 6. 7.
T4 (MEV)

Fig 22

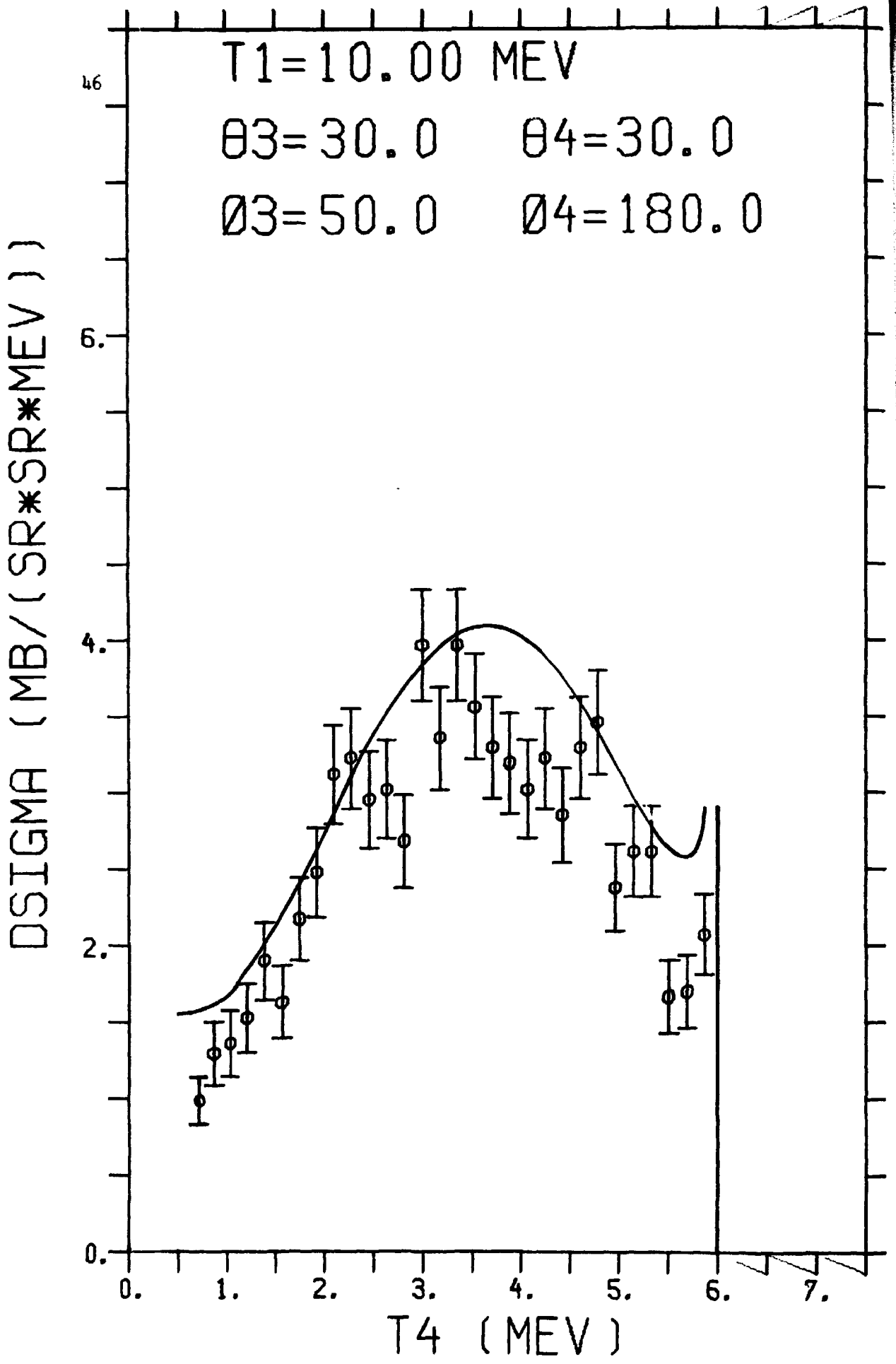
T1=10.00 MEV
θ3=30.0 θ4=30.0
Ø3=50.0 Ø4=180.0
DSIGMA (MB/(SR*SR*MEV))
0.
2.
4.
6.
0.
1.
2.
3.
4.
5.
6.
7.
T4 (MEV)

Fig 23

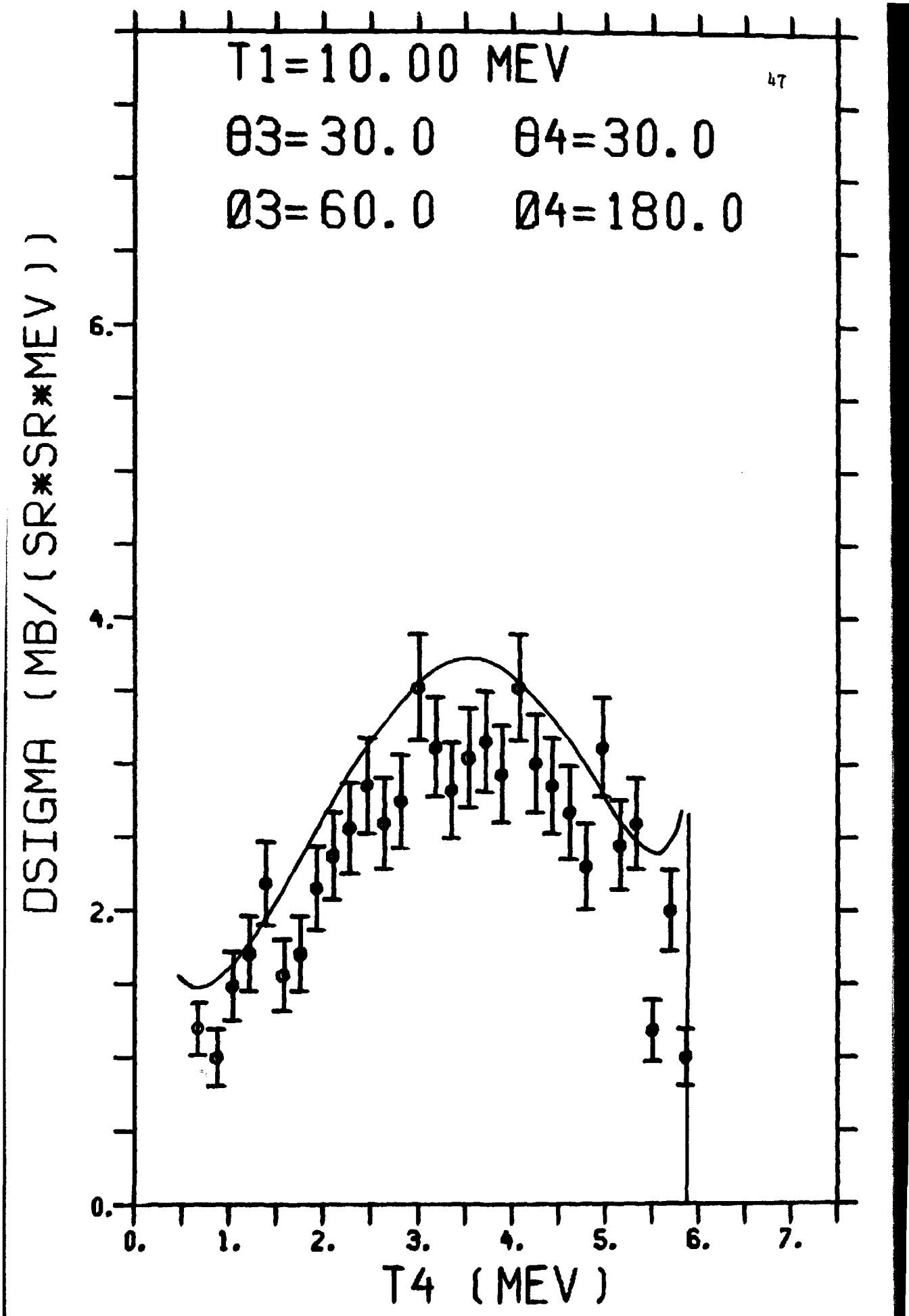
T1=10.00 MEV
θ3=30.0 θ4=30.0
Ø3=60.0 Ø4=180.0
DSIGMA (MB/(SR*SR*MEV))
0.
2.
4.
6.
0.
1.
2.
3.
4.
5.
6.
7.
T4 (MEV)

Fig 24

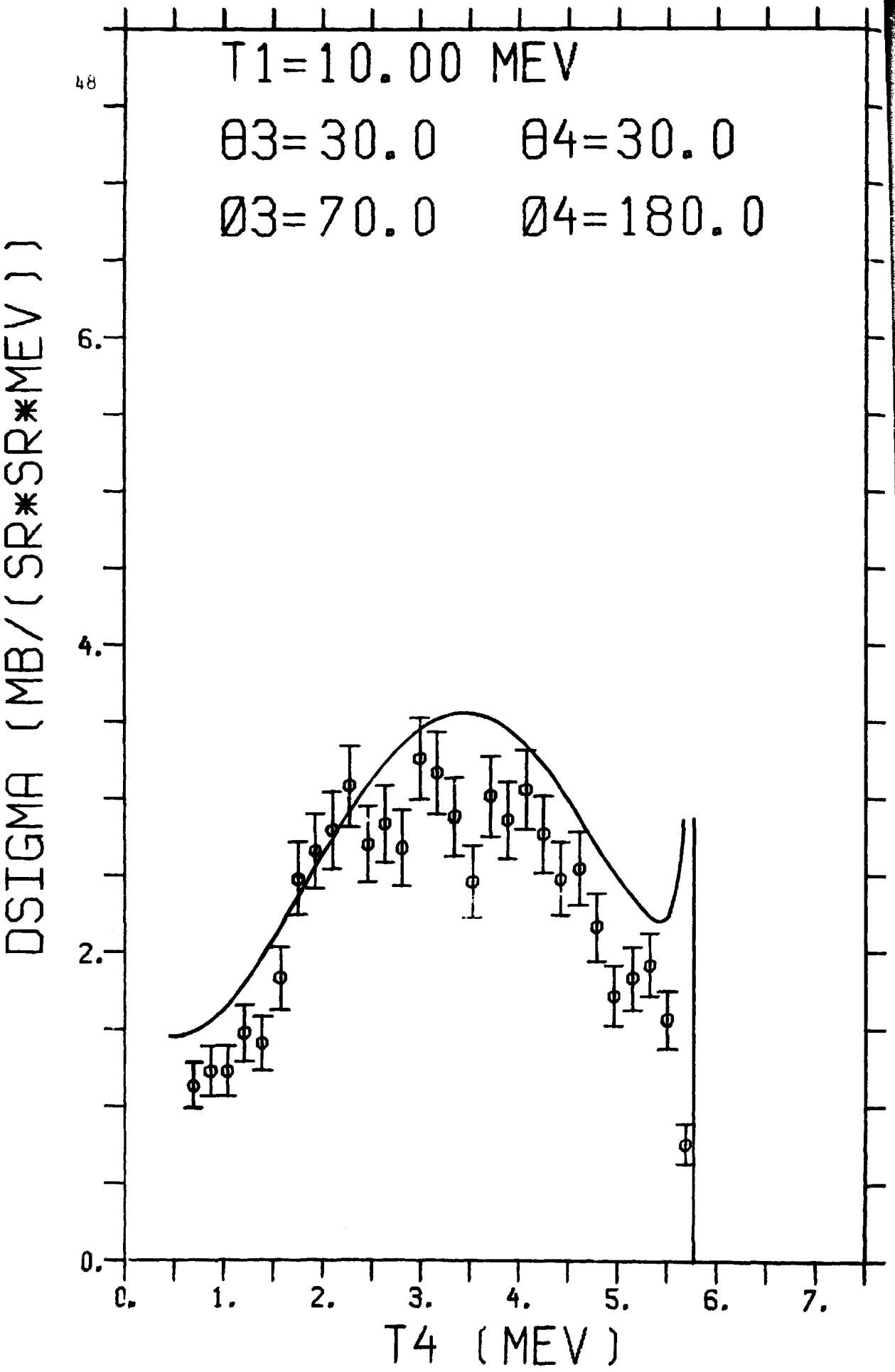
T1=10.00 MEV
θ3=30.0 θ4=30.0
Ø3=70.0 Ø4=180.0
DSIGMA (MB/(SR*SR*MEV))
0.
2.
4.
6.
0.
1.
2.
3.
4.
5.
6.
7.
T4 (MEV)

Fig 25

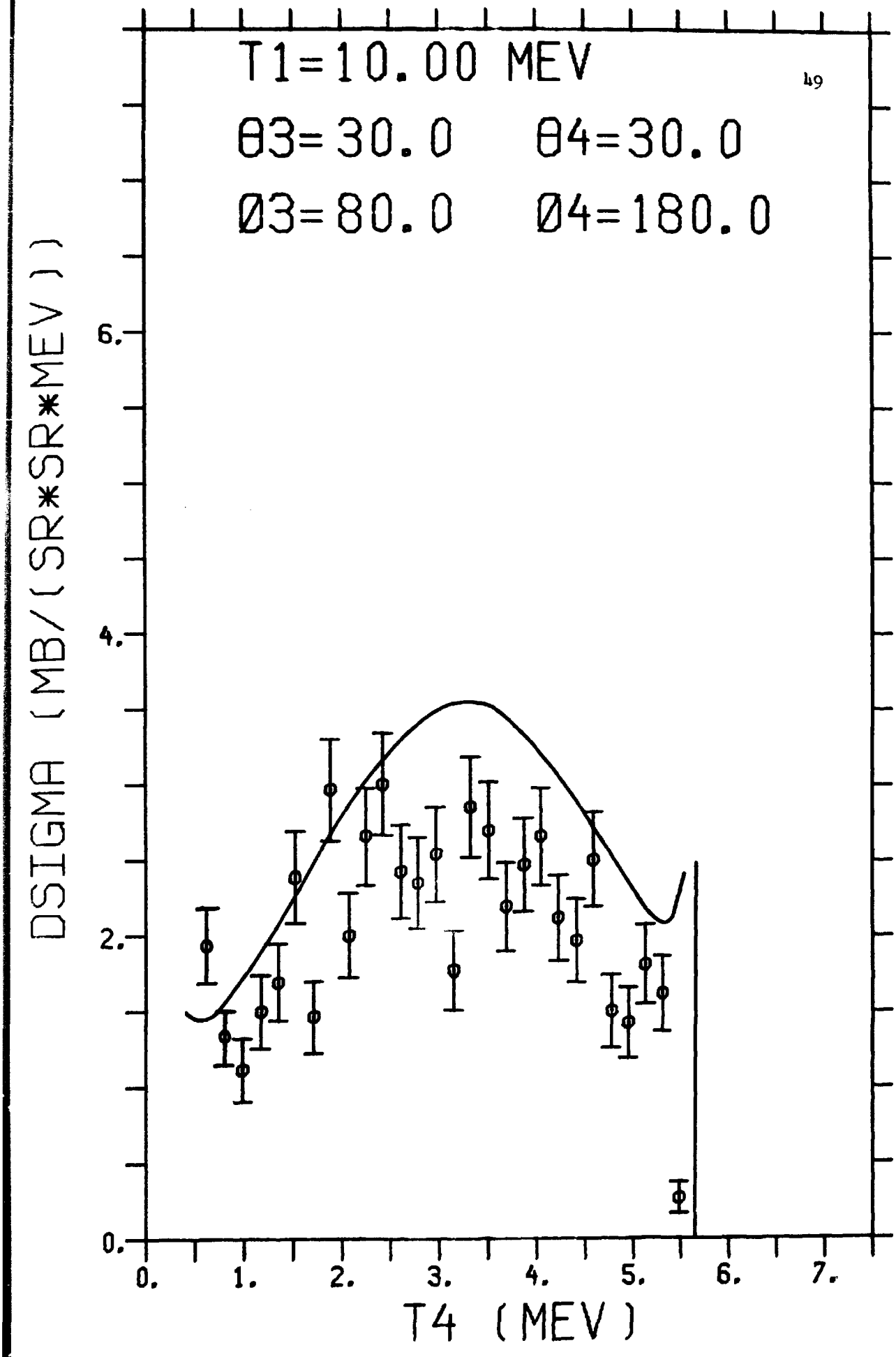
T1=10.00 MEV
θ3=30.0 θ4=30.0
Ø3=80.0 Ø4=180.0
DSIGMA (MB/(SR*SR*MEV))
0.
2.
4.
6.
0.
1.
2.
3.
4.
5.
6.
7.
T4 (MEV)

Fig 26

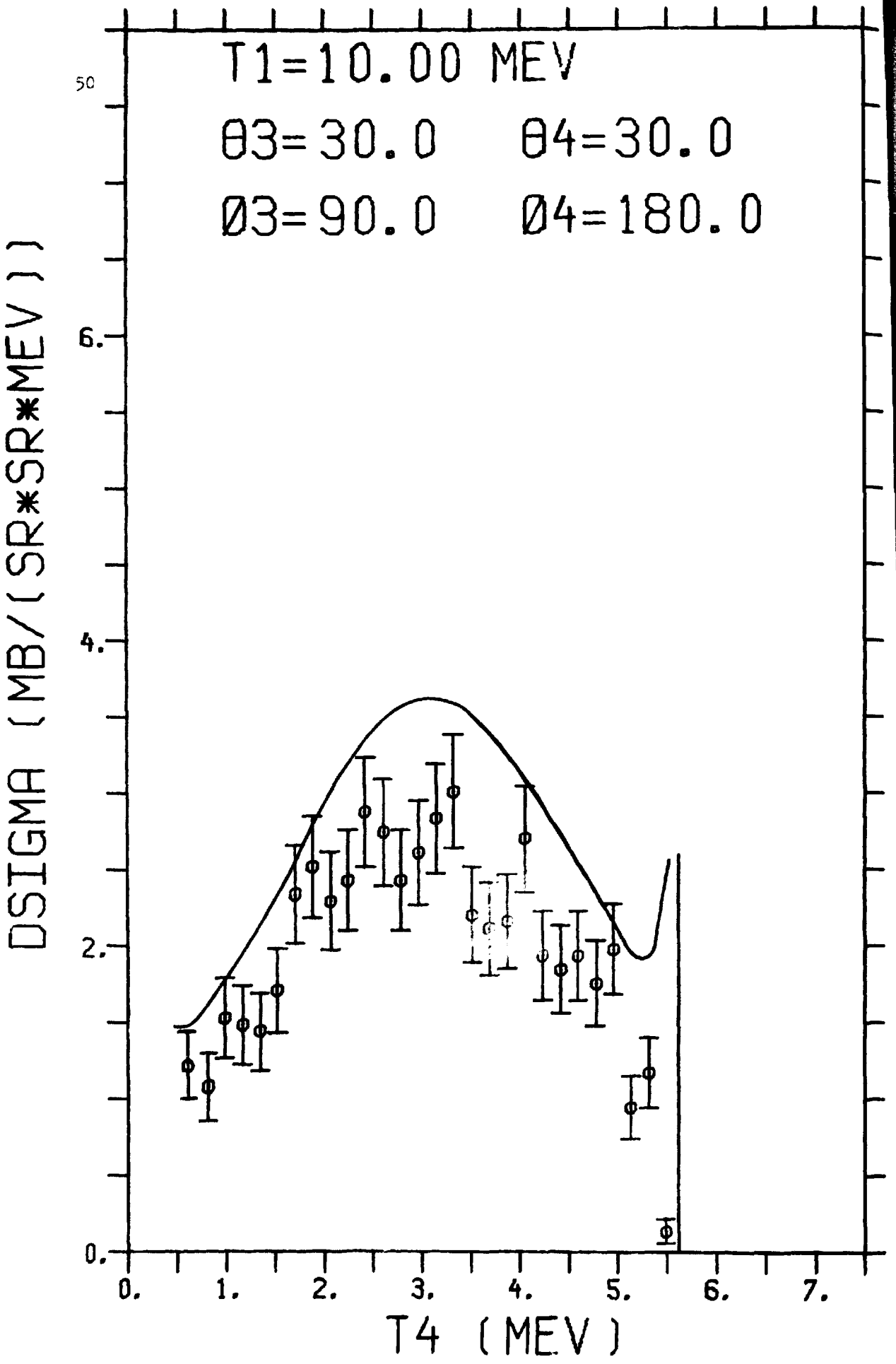
T1=10.00 MEV
θ3=30.0 θ4=30.0
Ø3=90.0 Ø4=180.0
DSIGMA (MB/(SR*SR*MEV))
50
6.
4.
2.
0.
0. 1. 2. 3. 4. 5. 6. 7.
T4 (MEV)

Fig 27

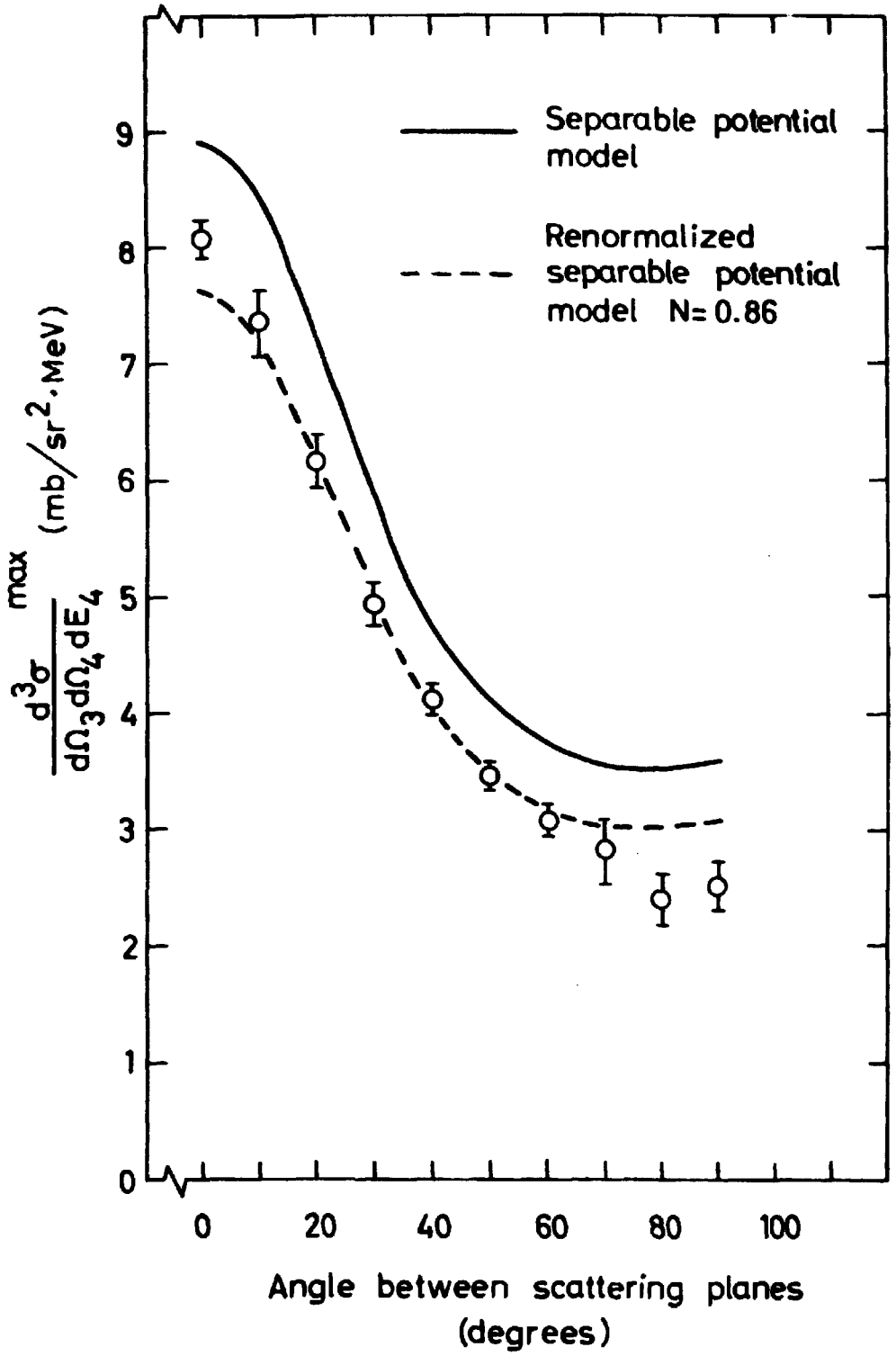
Separable potential model
Renormalized separable potential model N= 0.86
$\frac{d^3\sigma}{d\Omega_3 d\Omega_4 dE_4}^{max}$ (mb/sr^2.MeV)
0
1
2
3
4
5
6
7
8
9
0
20
40
60
80
100
Angle between scattering planes (degrees)

Fig 28

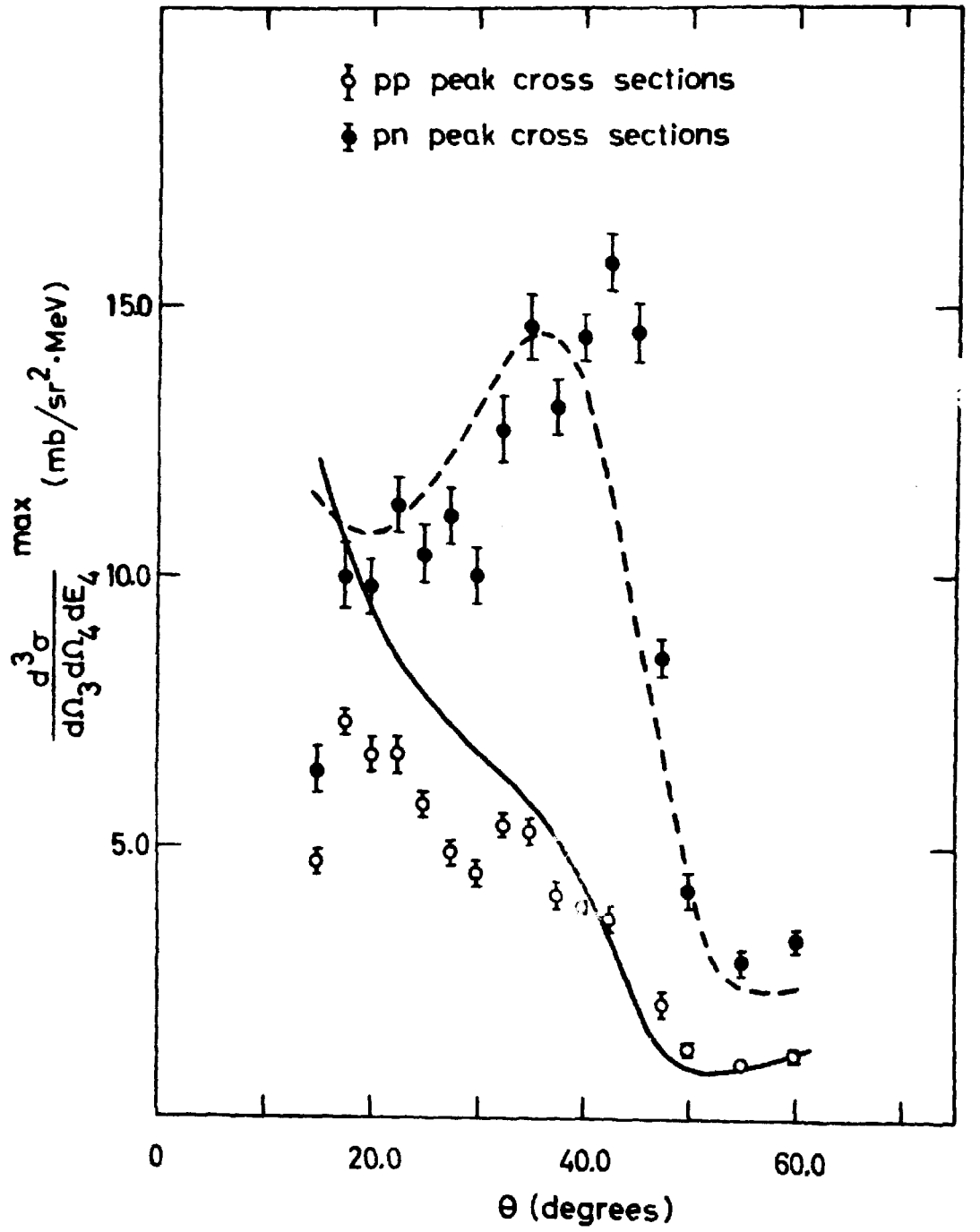
pp peak cross sections
pn peak cross sections
$\frac{d^3\sigma}{d\Omega_3 d\Omega_4 dE_4}^{max}$ (mb/sr^2·MeV)
15.0
10.0
5.0
0
20.0
40.0
60.0
θ (degrees)

Fig 29

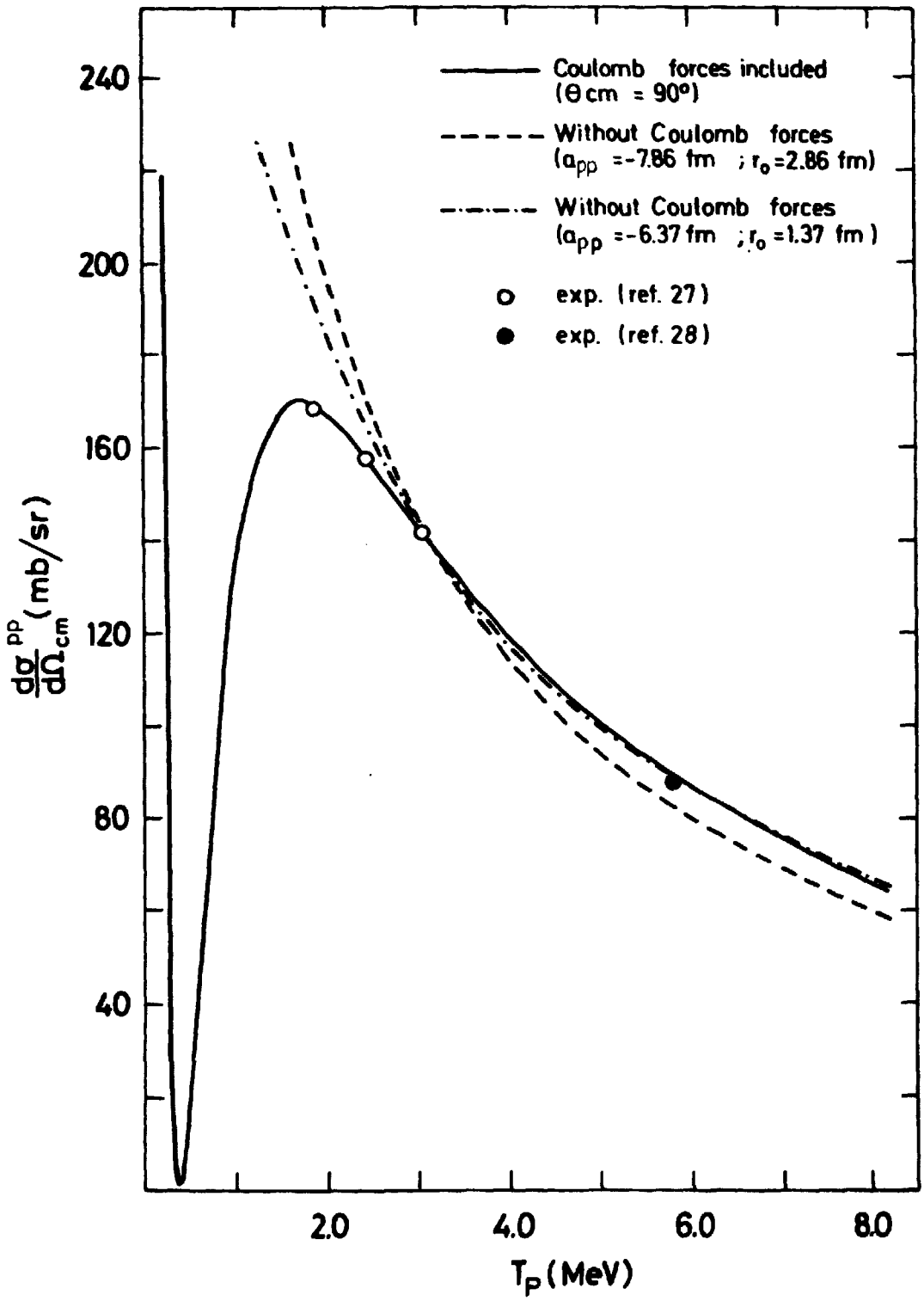
Coulomb forces included
(Θ cm = 90°)
Without Coulomb forces
(a_pp =-7.86 fm ; r_o =2.86 fm)
Without Coulomb forces
(a_pp =-6.37 fm ; r_o =1.37 fm)
exp. (ref. 27)
exp. (ref. 28)
240
200
160
120
80
40
2.0
4.0
6.0
8.0
T_p (MeV)
dσ/dΩ_cm^pp (mb/sr)

Fig 30